# Cell surface domain specific postsynaptic currents evoked by identified GABAergic neurones in rat hippocampus *in vitro*

Gianmaria Maccaferri, J. David B. Roberts, Peter Szucs, Carol A. Cottingham and Peter Somogyi

*MRC Anatomical Neuropharmacology Unit, Oxford University, Mansfield Road, Oxford OX1 3TH, UK*

(Received 21 October 1999; accepted after revision 11 January 2000)

1. Inhibitory postsynaptic currents (IPSCs) evoked in CA1 pyramidal cells ($n = 46$) by identified interneurones ($n = 43$) located in str. oriens were recorded in order to compare their functional properties and to determine the effect of synapse location on the apparent IPSC kinetics as recorded using somatic voltage clamp at −70 mV and nearly symmetrical [$Cl^-$].

2. Five types of visualised presynaptic interneurone, oriens-lacunosum moleculare (O-LMC), basket (BC), axo-axonic (AAC), bistratified (BiC) and oriens-bistratified (O-BiC) cells, were distinguished by immunocytochemistry and/or synapse location using light and electron microscopy.

3. Somatostatin immunoreactive O-LMCs, innervating the most distal dendritic shafts and spines, evoked the smallest amplitude ($26 \pm 10$ pA, S.E.M., $n = 8$) and slowest IPSCs (10–90% rise time, $6{\cdot}2 \pm 0{\cdot}6$ ms; decay, $20{\cdot}8 \pm 1{\cdot}7$ ms, $n = 8$), with no paired-pulse modulation of the second IPSC ($93 \pm 4$%) at 100 ms interspike interval. In contrast, parvalbumin-positive AACs evoked larger amplitude ($308 \pm 103$ pA, $n = 7$) and kinetically faster (rise time, $0{\cdot}8 \pm 0{\cdot}1$ ms; decay $11{\cdot}2 \pm 0{\cdot}9$ ms, $n = 7$) IPSCs showing paired-pulse depression (to $68 \pm 5$%, $n = 6$). Parvalbumin- or CCK-positive BCs ($n = 9$) terminating on soma/dendrites, BiCs ($n = 4$) and O-BiCs ($n = 7$) innervating dendrites evoked IPSCs with intermediate kinetic parameters. The properties of IPSCs and sensitivity to bicuculline indicated that they were mediated by $GABA_A$ receptors.

4. In three cases, kinetically complex, multiphasic IPSCs, evoked by an action potential in the recorded basket cells, suggested that coupled interneurones, possibly through electrotonic junctions, converged on the same postsynaptic neurone.

5. The population of O-BiCs (4 of 4 somatostatin positive) characterised in this study had horizontal dendrites restricted to str. oriens/alveus and innervated stratum radiatum and oriens. Other BiCs had radial dendrites as described earlier. The parameters of IPSCs evoked by BiCs and O-BiCs showed the largest cell to cell variation, and a single interneurone could evoke both small and slow as well as large and relatively fast IPSCs.

6. The kinetic properties of the somatically recorded postsynaptic current are correlated with the innervated cell surface domain. A significant correlation of rise and decay times for the overall population of unitary IPSCs suggests that electrotonic filtering of distal responses is a major factor for the location and cell type specific differences of unitary IPSCs, but molecular heterogeneity of postsynaptic $GABA_A$ receptors may also contribute to the observed kinetic differences. Furthermore, domain specific differences in the short-term plasticity of the postsynaptic response indicate a differentiation of interneurones in activity-dependent responses.

Interneurones releasing GABA are a major neuronal element in the cerebral cortex. Owing to its well laid out architecture, the hippocampus provides an attractive area to define the organisational principles and functional roles of interneurones exhibiting highly differentiated anatomical features (Ramon y Cajal, 1893). Distinct GABAergic cell types provide selective innervation of specific postsynaptic membrane domains of principal cells (Buhl *et al.* 1994; see Freund & Buzsaki, 1996; Somogyi *et al.* 1998) and express distinct neurochemical properties. Interneurones have been

implicated in a multitude of operational roles, such as: (i) feed-back, feed-forward and tonic somatic inhibition (Kandel *et al.* 1961; Andersen *et al.* 1963; Buzsaki & Eidelberg, 1981; Lacaille *et al.* 1987; Soltesz *et al.* 1995); (ii) control of dendritic calcium electrogenesis (Miles *et al.* 1996); (iii) regulation of dendritic backpropagation of action potentials (Buzsaki *et al.* 1996; Tsubokawa & Ross, 1996); (iv) regulation of synaptic plasticity; and (v) the regulation of network oscillations (Bragin *et al.* 1995; Cobb *et al.* 1995; Freund & Buzsaki, 1996).

It is not yet clear how the above-mentioned diverse roles of GABAergic cells may be related to the functional properties of the unitary postsynaptic responses that they generate in specific postsynaptic membrane domains. Particularly, the roles and receptor mechanisms of dendritic innervation remain uncertain. It has been suggested that different types of postsynaptic GABA receptors may be present on separate domains of the principal cells (Alger & Nicoll, 1982). Both $GABA_A$- and $GABA_B$-type synaptic responses have been recorded in pyramidal cells, but only $GABA_A$-type unitary IPSPs have been consistently evoked by single presynaptic interneurones (Miles & Wong 1984; Buhl *et al.* 1994; Ouardouz & Lacaille, 1997). Even the kinetics of $GABA_A$ receptor-mediated IPSCs are heterogeneous, suggesting a differential organisation of the underlying synapses (Pearce, 1993; Pearce *et al.* 1995; Banks *et al.* 1998). However, it has not been possible to correlate the different roles of interneurones and the observed synaptic response heterogeneity with the source of GABA from identified classes of interneurone.

The highly selective input and output relationships of distinct classes of interneurones provide the opportunity to compare the functional properties of unitary postsynaptic responses on functionally distinct domains of the same postsynaptic cell population. For the rigorous definition of the presynaptic interneurones, whole-cell electrophysiology, immunolabelling, and light and electron microscopy (EM) were employed. Our results underscore the importance of the identity of the presynaptic interneurone as a crucial factor in determining the functional properties of the postsynaptic effect.

## METHODS

### Slice preparation

The preparation of hippocampal slices was carried out as described by Maccaferri & McBain (1996). Young rats (Wistar, age P10–P17) were deeply anaesthetized using isoflurane and killed by decapitation. In a few experiments cervical dislocation (Schedule 1 procedure, The Animals (Scientific Procedures) Act) was used to kill the animal. The brain was quickly removed and placed into ice-cold artificial cerebrospinal fluid (ACSF) of the following composition (mM): 130 NaCl, 24 $NaHCO_3$, 3·5 KCl, 1·25 $NaH_2PO_4$, 1 $CaCl_2$, 3 $MgSO_4$ and 10 glucose, saturated with 95% $O_2$, 5% $CO_2$, at pH 7·4. The hemisected brain was then glued onto the stage of a vibrating microtome (Leica, Germany) and sections of 300 $\mu$m thickness were cut and stored in an incubation chamber at room temperature for about 1 h before use.

Both pyramidal cells and str. oriens/alveus interneurones were identified visually as potential targets using a Zeiss Axioskop microscope (Zeiss, Germany) equipped with a ×40 immersion DIC objective coupled with an infrared camera system (Hamamatsu, Japan). Pyramidal cells selected for recordings were usually located at the border between str. pyramidale and str. oriens; interneurones were usually selected for their elongated appearance, parallel to str. pyramidale as described by Maccaferri & McBain (1995).

### Electrophysiological recording

Conventional whole-cell recordings were applied. Pyramidal cells were voltage clamped at a holding potential of −70 mV using an Axopatch-1D amplifier (Axon Instruments) and a pipette of ∼2 MΩ resistance. The solution used to fill the electrodes consisted of (mM): 100 CsCl, 2 $MgCl_2$, 0·1 EGTA, 2 ATP, 0·3 GTP, 40 Hepes, 5 QX-314 and 0·5% biocytin at pH 7·2. The standard recording solution was composed of (mM): 130 NaCl, 24 $NaHCO_3$, 3·5 KCl, 1·25 $NaH_2PO_4$, 3 $CaCl_2$, 1·5 $MgSO_4$ and 10 glucose, saturated with 95% $O_2$, 5% $CO_2$, at pH 7·4. Mean series resistance in the postsynaptic cell was 12·8 ± 0·7 MΩ ($n = 45$, S.E.M.) and routinely compensated to ∼80%.

Str. oriens/alveus interneurones were kept under current-clamp configuration with an EPC7 amplifier (List, Germany); spontaneous rhythmic firing (Maccaferri & McBain, 1996) was prevented by injection of a tonic hyperpolarizing current. The intracellular solution was different from the one used for pyramidal cell recording and consisted of (mM): 130 potassium gluconate, 2 $MgCl_2$, 0·1 EGTA, 2 ATP, 0·3 GTP and 10 Hepes, as well as 0·5% biocytin at pH 7·2. In a few experiments KCl was used instead of potassium gluconate, without obvious difference in the results, and therefore the data were pooled. All recordings were performed at ∼30 °C, as measured in the superfusion fluid. The temperature was set at 35 °C via a Peltier device connected to the recording chamber (Luigs & Neumann, Germany) and monitored via a thermometer applied to the metal frame supporting the recording chamber. IPSC records were obtained by eliciting action potentials in the interneurone at 0·1–1 Hz by injection of a suprathreshold square current pulse. In experiments regarding short-term plasticity, pairs of action potentials were elicited in the presynaptic interneurone at 0·2 Hz. Only stable recordings from pairs of synaptically connected cells were included in the study.

### Data analysis

Data were recorded on a DAT recorder (Biologic, France), filtered at 5 kHz and digitised at ∼20 kHz using a Digidata 1200 A/D board. Analysis was performed using the pCLAMP and Origin software packages (Axon Instruments and Microcal Software, Northampton, MA, USA, respectively) and the Whole Cell Program (courtesy of Dr J. Dempster, University of Strathclyde, UK). Because of the very high frequency of spontaneous IPSCs, recordings were carefully selected after visual inspection of individual traces in order to discard obviously distorted records. Single sweep IPSCs were averaged after alignment using the presynaptic spike as trigger. Spike triggering was not used for the alignment of IPSCs generated by long trains of action potentials, except for the comparison of IPSCs evoked by the first and the last action potential of the train. Amplitudes of unitary IPSCs (uIPSCs), or noise for histograms were measured in a 0·5–1 ms time window corresponding to the peak of the response of the averaged IPSC, or in a 0·5–1 ms window of the baseline preceding the IPSC, respectively. Stationarity of the IPSC amplitude was routinely checked before building histograms and for the double pulse analysis. In case some run-down of the IPSCs occurred, the consistency of paired-pulse modulation was checked throughout the

period selected for the analysis. For all other purposes, amplitudes of averaged IPSCs were measured with cursors using the aforementioned programs. Averaged uIPSCs were obtained from 70 ± 7 traces (mean ± S.E.M.) (range 8–212) for kinetic analysis and 114 ± 10 traces (range 8–254) for amplitude analysis. The decay phase of the uIPSCs was fitted by either mono- or biexponential equations: the time constant of the monoexponential fit or the weighted average of the two time constants obtained from biexponential fits (Banks *et al.* 1998) was used for the analysis. In two cases, where neither mono- or biexponential functions could adequately fit the decay of the IPSC, the time to 63% of decay was used. Unless otherwise stated, statistical comparison of IPSC properties was performed using Student's $t$ test for two independent populations. Data are presented as means ± S.E.M.

Analysis of IPSCs presented in Figs 9 and 11 was performed by visually inspecting inflections in each single sweep trace following the uIPSC. Inflections were counted in 1 ms bins corresponding to their time of onset after the unitary IPSC. The mean number of expected inflections per bin, due to spontaneous background activity, was calculated from a 25–50 ms interval beginning 50 ms after the onset of the uIPSC. The probability that the measured number of events could arise by chance could then be calculated on the basis of the expected events using Poisson statistics.

**Visualisation of recorded cells and anatomical evaluation**

The slices were sandwiched between two Millipore filters to avoid deformations and fixed for 1–7 days in a solution containing 2·5% paraformaldehyde, 1·25% glutaraldehyde and 15% (v/v) saturated picric acid in 0·1 M phosphate buffer (pH 7·4). Following gelatine embedding, the slices were re-sectioned at 60 $\mu$m thickness and the biocytin-filled cells were visualised by the avidin-biotinylated horseradish peroxidase method with 0·05% diaminobenzidine as chromogen and 0·01% $H_2O_2$ as substrate for peroxidase. Sections were postfixed in 1% $OsO_4$ and block stained in 1% uranyl acetate, dehydrated and embedded into epoxy resin (Durcupan, Fluka) on glass slides.

Recovered cells were reconstructed from the serial 60 $\mu$m thick sections under a light microscope using a drawing tube from the entire slice, unless otherwise stated. Following light microscopic analysis, axon-rich areas, including all layers covered by the axonal field, were cut out from the thin layer of resin on the slide and re-embedded for ultrathin sectioning. Serial sections were cut and mounted on single-slot pioloform-coated copper grids. The sections were scanned in the electron microscope and all biocytin-filled axonal profiles, which formed synaptic junctions, were photographed. Since all profiles were followed and the plane of the section randomly cuts through the axonal branches, the above procedure ensured a random sample of postsynaptic targets and provides an objective basis for cell classification (see Somogyi *et al.* 1998). Postsynaptic somata, axon initial segments, dendritic shafts and spines were identified on published criteria (Peters & Palay, 1996). In brain slices incubated *in vitro*, some structural features change with incubation time. The microtubule fascicles of axon initial segments (AISs) are rarely seen in slices from young animals. Therefore, the electron dense undercoating, frequent coated pits and accumulated large vesicles were used for identification. Even so, in some cases, the decision as to whether a postsynaptic element was an AIS or a dendrite could not be made and these profiles are presented as unidentified (Table 2). Larger dendrites always contain mitochondria and microtubules and are easily recognized. Small diameter postsynaptic profiles containing mitochondria and/or microtubules were classified as dendritic shafts; those lacking both structures were considered dendritic spines. In some cases it could not be determined whether a small postsynaptic profile was a dendritic shaft or spine and these are listed as unidentified structures (Table 2). In addition to the postsynaptic membrane specialization when present, we verified synaptic junctions based on the following criteria: (i) vesicle accumulation in the presynaptic axonal varicosity; (ii) rigid membrane apposition between the pre- and postsynaptic element with a characteristic widening of the extracellular space; (iii) electron opaque cleft material, when not obscured by the peroxidase reaction product. When the plane of the section was tangential to the junctional membranes, the synaptic cleft could be recognized by tilting the section using the goniometer of the electron microscope.

**Immunocytochemistry of perfusion fixed brain sections**

Immunoreactivity for somatostatin was examined in the hippocampus of one adult (150 g) and one developing (P13) Wistar rat. The animals were deeply anaesthetised (Sagatal, pentobarbitone sodium, 220 mg $kg^{-1}$ I.P.) and killed by perfusion, first with saline, followed by a fixative of 4% paraformaldehyde, 0·05% glutaraldehyde and 15% (v/v) saturated picric acid in 0·1 M phosphate buffer (pH 7·4). The brains were dissected, and 70 $\mu$m thick Vibratome sections were cut. The sections were washed in PBS, and non-specific protein binding was blocked by incubation in normal goat serum for 1 h, followed by incubation with monoclonal antibodies to somatostatin (code SOMA8, gift from A. Buchan, University of British Columbia, ascites fluid diluted 1:500 in TBS, 0·1% Triton X-100). The sections were further incubated for 2 h in a solution of fluorescein (FITC)-conjugated goat anti-mouse IgG (diluted 1:100, Jackson ImmunoResearch Laboratories, West Grove, PA, USA).

**Immunocytochemistry on brain slices**

For the neurochemical characterisation of non-pyramidal cells, some cells were tested by immunocytochemistry, but owing to the use of detergent, only some of them could be analysed in the electron microscope as described above. All slices for immunocytochemistry were fixed in 2·5% paraformaldehyde, 0·05% glutaraldehyde and 15% (v/v) saturated picric acid in 0·1 M phosphate buffer (pH 7·4) for 2 h, followed by washing in PBS. Non-specific protein binding was blocked by incubation in normal goat serum for 1 h. Monoclonal antibodies to somatostatin (code SOMA8, ascites fluid diluted 1:500), characterised as recognising somatostatin and SOM-28, were mixed with previously characterised rabbit polyclonal antibodies to parvalbumin (kindly provided by Dr K. G. Baimbridge, University of British Columbia, diluted 1:250), or with commercial rabbit antibodies to parvalbumin (Swant, Switzerland, code PV-28, diluted 1:250). In other experiments monoclonal antibodies to parvalbumin (Sigma, code P3171, diluted 1:250), reported as recognising only parvalbumin, were used mixed with rabbit polyclonal antibodies to the C-terminal nonapeptide (107–115) of rat pro-cholecystokinin (diluted 1:1000, Morino *et al.* 1994). The antibodies were diluted in Tris-buffered saline, in some cases containing 0·1% Triton X-100, and applied overnight. The sections were subsequently washed in TBS and incubated for 2 h in a mixture of fluorescein (FITC)-conjugated goat anti-mouse IgG (diluted 1:100, Jackson ImmunoResearch), Cy3-conjugated goat anti-rabbit IgG (diluted 1:200, Jackson ImmunoResearch) and 7-amino-4-methylcoumarin-3-acetic acid (AMCA)-conjugated streptavidin (diluted 1:1000, Vector Laboratories, Burlingame, CA, USA). Biocytin-filled cells were studied using a Leica dichromatic mirror system and the A4 filter block (excitation filter, BP 360/40 nm, reflection short pass filter (RKP) 400 nm, suppression filter LP 470/40 nm) for visualising AMCA, the L5 block (excitation filter, BP 480/40 nm, RKP 510 nm, suppression filter BP 527/30 nm) for recording FITC fluorescence and the Y3 block

**Table 1. Classification of interneurones based on axonal and dendritic patterns, postsynaptic targets and neuropeptide content**

| | Interneurone type | | | | | | | |
|---|---|---|---|---|---|---|---|---|
| | | | Bistratified | | | | | |
| | O-LM | Basket | Radial BiC | O-BiC | Axon only | Axo-axonic | Unident-ified | Total |
| No. of cells | 8 | 9 | 4 | 7 | 1 | 6 | 8 | 43 |
| Somatostatin immunoreactivity (positive; tested) | 5; 6 | 0; 4 | 1; 2 | 4; 4 | — | 0; 3 | — | 10; 19 |
| Cholecystokinin immunoreactivity (positive; tested) | — | 1; 4 | 0; 1 | 0; 2 | — | — | — | 1; 7 |
| Parvalbumin immunoreactivity (positive; tested) | 1; 2 | 1; 2 | 0; 1 | 1; 3 | — | 2; 3 | — | 5; 11 |
| No. of cells analysed by electron microscopy | 1 | 5 | — | 2 | — | 6 | — | 14 |
| No. of synaptic junctions in random EM sample | 14 | 65 | — | 33* | — | 62 | — | 174* |
| No. of recorded postsynaptic pyramidal cells | 8 | 10 | 4 | 8 | 1 | 7 | 8 | 46 |

Where no value is given, the cell was not tested or the test not applicable. * Four boutons were from an axon collateral *selected* within the pyramidal layer, and they made synapses only with dendrites.

(excitation filter, BP 535/50 nm, RKP 565 nm, suppression filter BP 610/75 nm) for recording Cy3 fluorescence. Cells were recorded on a CCD camera, analysed and displayed using the Openlab software (Improvision, Coventry, UK). Brightness and contrast were adjusted for the whole frame, and no part of a frame was enhanced or modified in any way. The immunonegativity of a cell for a marker could be due to damage caused by the recording, an undetectably low level of the molecule or the genuine absence of the molecule, and therefore only the positive detection of immunoreactivity is informative following extensive whole-cell recording. The recorded cells usually showed significantly lower immunoreactivity than nearby unrecorded cells, suggesting that the recording decreased the somatic level of the peptides.

Following immunocytochemical testing, the sections were removed from the slides, washed in PBS and processed for peroxidase-based visualisation of the recorded cells for reconstruction of the axonal and dendritic patterns and permanent storage. The sections were incubated in biotinylated horseradish peroxidase (diluted 1:100, Vector Laboratories) before further washing and incubation in avidin–biotinylated-horseradish peroxidase complex (diluted 1:100, Vector Laboratories) and peroxidase enzyme reaction as described above. Some of the immunocytochemically characterised cells which were not incubated in detergent were also studied in the electron microscope.

Primary antibody specificity has been reported previously. Method specificity was tested for all three antibodies by replacing the primary antibodies with 1 % normal serum from the same species. Method specificity was tested for the antibodies to somatostatin by preincubating the antibody with $10^{-5}$ M somatostatin (Sigma) for 5 h at room temperature before applying the mixture to the sections. This completely prevented immunolabelling. Immunolabelling with the antibody to pro-CCK was reported to be abolished by preadsorption to the synthetic nonapeptide (Morino *et al.* 1994). When one of the secondary antibodies was omitted following application of primary antibodies from two species, no immunolabelling was detected in the colour of the omitted antibody, showing that each filter block only allowed detection of the appropriate secondary antibody at the intensity of labelling used in the present study. From these control experiments we conclude that the labelling detected in each colour was due to the selective binding of the primary antibodies.

**Selection criteria and cell identification**

From a large sample of simultaneous, double whole-cell recordings in the hippocampus, 46 synaptically connected interneurone to pyramidal cell pairs were selected (Table 1). The total number of presynaptic interneurones recorded was 43, because in three cases the postsynaptic effect of the interneurone was tested on two sequentially recorded pyramidal cells. The basis of selection was: (i) presence of a short latency IPSC in the pyramidal cell following an action potential in the putative interneurone; (ii) stable recordings from both cells for sufficient time to obtain an averaged IPSC; and (iii) recovery of at least a part of a biocytin-labelled interneurone. In 30 paired recordings, the soma, dendrites and axon of the interneurone were recovered, in 10 cases only the axon, in one case the soma and the axon, and in three cases only the axon and some dendrites were visualised by biocytin. Overall, the success of recovering some anatomical information about the recorded interneurones was about the same as with sharp electrode recordings in previous studies (Buhl *et al.* 1994). The postsynaptic pyramidal cell was also recovered in 36 cases to a varying degree. However, in most cases the pyramidal cell dendritic tree was poorly revealed due to the use of large-diameter, low-resistance (~2 MΩ) whole-cell electrodes, resulting in poor sealing of the membrane and a collapse of the cell following withdrawal of the electrode. Only in six cases were both the pyramidal cell and the interneurone sufficiently recovered to evaluate the putative contact sites between the interneurone axon and the pyramidal cell and three of these cases are illustrated (Figs 2, 4 and 8*A*).

Interneurones were provisionally classified on the basis of the layer specific distribution of their axon (Ramon y Cajal, 1893; Buhl *et al.* 1994; McBain *et al.* 1994; Freund & Buzsaki, 1996). Subsequently, 14 cells were tested by EM for the unequivocal identification of their postsynaptic target distribution. Cells were analysed by electron microscopy when the light microscopic assessment left doubt about the postsynaptic target domain due to the laminar overlap of functionally distinct domains, e.g. somata and axon initial segments, or somata and dendrites. In the other cases, namely for an O-LM cell and for a group of bistratified cells (O-BiC), the EM analysis was carried out because quantitative characterisation had not been reported at the time of our study. In addition, immunocytochemical reactions were carried out on 20 cells in the present sample. Five different classes of presynaptic interneurones could be identified

**Table 2. Electron microscopic characterisation of postsynaptic targets of identified interneurones**

| | | | Percentage postsynaptic targets | | | | |
|---|---|---|---|---|---|---|---|
| Cell no. | Cell type | No. of targets tested | Axon i. segment | Spine | Dendrite | Soma | Unident-ified |
| 070198SL22 | O-LM | 14 | 0 | 29 | 57 | 0 | 14 |
| 100898SL56 | O-Bistratified | 16 | 0 | 19 | 69 | 0 | 13 |
| 130298SL36 | O-Bistratified | 17 | 0 | 0 | 82 | 12 | 6 |
| 250298SL38 | Axo-axonic | 9 | 78 | 0 | 0 | 0 | 22 |
| 280499SL67 | Axo-axonic | 11 | 100 | 0 | 0 | 0 | 0 |
| 290499SL70 | Axo-axonic | 11 | 91 | 0 | 0 | 0 | 9 |
| 150599SL76 | Axo-axonic | 10 | 80 | 0 | 0 | 0 | 20 |
| 120599SL80 | Axo-axonic | 9 | 100 | 0 | 0 | 0 | 0 |
| 110599SL79 | Axo-axonic | 12 | 83 | 0 | 0 | 0 | 17 |
| 260499SL64 | Basket | 13 | 0 | 0 | 62 | 38 | 0 |
| 280499SL66 | Basket | 14 | 0 | 0 | 64 | 36 | 0 |
| 110599SL78 | Basket | 10 | 0 | 0 | 30 | 70 | 0 |
| 090398SL42 | Basket | 16 | 0 | 0 | 63 | 25 | 13 |
| 140599SL83 | Basket | 12 | 0 | 0 | 50 | 42 | 8 |
| Total: 14 | | 174 | | | | | |

based on their efferent postsynaptic target domain (Table 1). (i) Oriens-lacunosum moleculare cells (O-LMCs), targeting distal dendrites in str. lacunosum-moleculare. Although they frequently had local axon collaterals in str. oriens (Fig. 3*C*), as also reported from more extensive *in vivo* labelling (Sik *et al.* 1995), the vast majority of the terminals of the axonal arborization of O-LM cells are located in str. lacunosum-moleculare (Ramon y Cajal, 1893, his Fig. 8, cell a; McBain *et al.* 1994; Sik *et al.* 1995; Maccaferri & McBain, 1995, 1996; Ali & Thomson, 1998; Katona *et al.* 1999). (ii) Oriens-bistratified cells (O-BiCs), defined in this study as having horizontal dendrites in str. oriens/alveus and targeting mainly pyramidal dendrites in str. oriens and radiatum. (iii) Bistratified cells (BiCs), having radial dendrites and an axon targeting the dendrites of pyramidal cells located in str. oriens and radiatum and rarely also somata (Buhl *et al.* 1994; Sik *et al.* 1995; Ali *et al.* 1998). (iv) Basket cells (BCs), targeting soma and proximal dendrites with an axon centred on str. pyramidale (Ramon y Cajal, 1893; Buhl *et al.* 1994; Sik *et al.* 1995). And (v) axo-axonic cells (AACs), targeting pyramidal cell axon initial segments (Somogyi *et al.* 1998).

## RESULTS

During complete blockade of fast glutamatergic synaptic transmission by bath application of 6,7-dinitro-quinoxaline-2,3-dione (DNQX; 20 $\mu$M) and D(−)2-amino-5-phosphono-pentanoic acid (D-AP5; 50 $\mu$M), generation of action potentials in the presynaptic interneurone was followed by a postsynaptic current in the connected pyramidal cell held under voltage clamp at −70 mV. In all cases, due to the high [$Cl^-$] of the pipette solution, the recorded IPSCs were inward currents, consistent with anionic currents flowing through synaptically activated $GABA_A$-type receptors.

In 36 out of 43 presynaptic interneurones it was possible unambiguously to identify the class of the recorded cells on the basis of the anatomical analysis; in the other seven cases the amount of interneurone axon recovered was insufficient for classification. The innervation of four domains of pyramidal cells by distinct classes of presynaptic interneurones is presented in a distal to proximal order.

### O-LM interneurones

The postsynaptic effect of eight O-LM cells on pyramidal neurones was investigated (Figs 1*A* and 2*C*). In response to a single presynaptic action potential the connections could be highly reliable without apparent response failures (Fig. 1*B* and *C*, $n = 143$). Analysis of the IPSC amplitude distribution resulted in a unimodal distribution of events, well separated from the background noise (Fig. 1*B*). In this case, the number of potential synaptic contact sites could not be determined owing to the partial visualisation of the axon. In other cases, however, the detection of the postsynaptic effect was much less reliable and averaging of several individual sweeps was needed to unmask an IPSC. In the reconstruction shown in Fig. 2, despite the light microscopic identification of 17 possible synaptic sites (Fig. 2*B*) the postsynaptic effect was very small (Fig. 2*C*). In another fully reconstructed case (not shown) only three potential contact sites were found, all in str. lacunosum-moleculare. On average, the amplitude of the somatically recorded uIPSCs evoked by O-LM cells was $26 \pm 10$ pA ($n = 8$), the smallest amplitude uIPSC as compared to those evoked by other types of cell recorded in our sample (see below).

The distinctive firing pattern of O-LM interneurones (Fig. 1*C*) has been reported previously (Ali & Thomson, 1998) and is similar to that described for somatostatin-immunopositive interneurones in the rat neocortex (Reyes *et*

*al.* 1998). These cells have been shown to display regular spontaneous firing at frequencies between 5 and 7 Hz *in vitro* (Maccaferri & McBain, 1996) due to their intrinsic membrane properties. Although there are no direct data on the firing rate of identified O-LM interneurones *in vivo*, the situation could be similar, because the average firing rate of unidentified interneurones located in str. oriens/alveus has been reported to be around 10 Hz (Csicsvari *et al.* 1999). Therefore, we used this frequency of presynaptic spikes to test the effect of repetitive O-LM cell activation on the postsynaptic IPSC with a paired-pulse protocol (Fig. 1*D*). Little change of the second IPSC was elicited at either 100 ms (4·4 % depression) or 50 ms (15·4 % depression, data not shown) interpulse interval. The response to prolonged repetitive firing with brief interspike intervals, evoked by a depolarizing current pulse, showed an initial summation followed by a period of somewhat diminished IPSC amplitude (Fig. 1*C*). The level of the postsynaptic current at the end of the spike train, however, was similar to the amplitude of the peak of the IPSC generated by the first spike.

The stratum oriens and alveus border region contains a high density of somatostatin immunoreactive GABAergic cells (Somogyi *et al.* 1984; Katona *et al.* 1999). After recording, six O-LM interneurones were tested for somatostatin immunoreactivity and in five cases the interneurones were clearly immunopositive (Fig. 3*A* and *B*), whereas in the remaining case the result was inconclusive. The strength of immunoreactivity in the recorded cell was usually lower than in the neighbouring cells, probably due to the decrease of peptide synthesis and/or increase in degradation in the dialysed cell. Therefore, negative immunocytochemical results cannot be taken as evidence for the absence of expression of the peptide by any of the recorded cells. Somatostatin immunoreactivity was mostly located in the perinuclear area and in the proximal dendrites in granules and in patches corresponding to the Golgi apparatus (Fig. 3*B*). One of two somatostatin-positive O-LM cells tested was weakly immunopositive for parvalbumin.

A random sample of electron microscopically tested axonal branches of an O-LM cell showed that the postsynaptic targets were dendritic shafts and spines in str. lacunosum-moleculare (Fig. 3*D* and *E*, Table 2), confirming recently reported quantitative results for somatostatin immunoreactive terminals (Katona *et al.* 1999) and qualitative

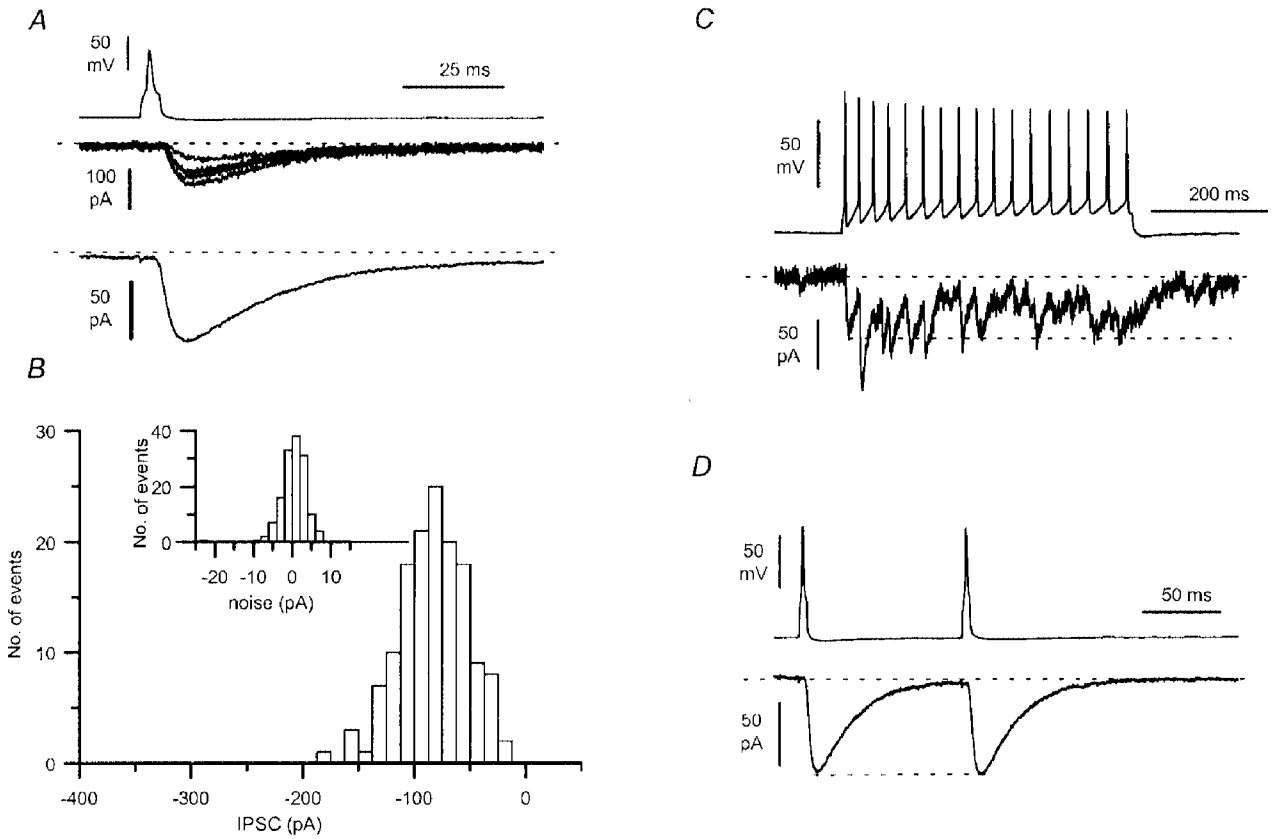


**Figure 1. Postsynaptic effect of a somatostatin-immunopositive O-LM interneurone**

*A*, unitary IPSCs in a pyramidal cell (single sweeps and the average of 49 traces) evoked by single presynaptic action potentials (P14 animal, see also Fig. 3). *B*, peak amplitude distribution of the uIPSCs ($n = 143$) and noise (inset). *C*, the firing pattern of the presynaptic interneurone following the injection of a current step (200 pA amplitude, 500 ms duration) shows a small degree of accommodation and a decrease of action potential amplitude during the train. Note the fusion of the postsynaptic response and the similar current level at the peak of the first IPSC and at the end of the train (dashed line). *D*, paired action potentials at 100 ms interspike intervals evoked IPSCs of very similar amplitude (average of 49 sweeps).

results obtained from an *in vivo* recorded cell (Sik *et al.* 1995). Some of the synaptic junctions were exceptionally large (Fig. 3*E*); others were small puncta made by the axon collateral without forming a varicosity. It would therefore be very difficult to estimate the total number of synapses made by an O-LM cell on the basis of light microscopy. Due to the laminar preference of the terminals, the synapses of GABAergic O-LM cells in str. lacunosum-moleculare are in proximity to the lamina specific excitatory inputs from the thalamus and the entorhinal cortex. Indeed, electrophysiological experiments have suggested that O-LM cells can regulate the gain of EPSPs on pyramidal cell distal dendrites (Maccaferri & McBain, 1995).

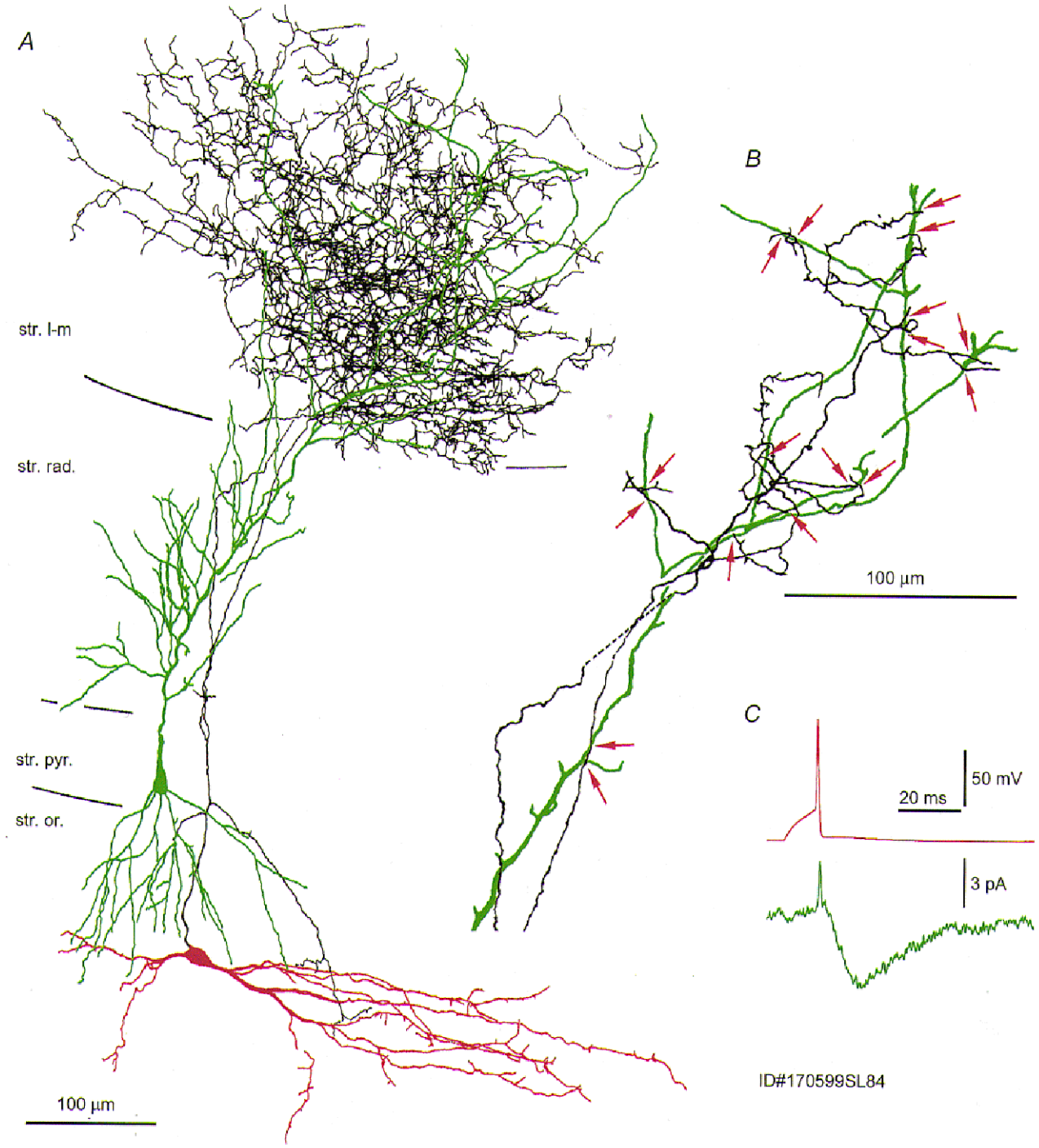


**Figure 2. Reconstruction of a somatostatin-immunopositive O-LM to pyramidal cell pair**

*A*, extensive overlap between the distal dendrites of the pyramidal cell (green) and the interneurone axon (black) at P15. The soma and dendrites of the interneurone are shown in red. *B*, light microscopic analysis revealed seventeen axon to dendrite close appositions (red arrows). *C*, the somatically recorded postsynaptic current in the pyramidal cell was very small (cf. Fig. 1).

**Bistratified cells**

Bistratified cells were originally defined on the basis of a dense axonal plexus in str. radiatum and oriens, leaving str. pyramidale only sparsely crossed by axons, and a postsynaptic target profile of dendritic shafts and spines with only occasional synapses given to somata (Buhl *et al.* 1994; Sik *et al.* 1995; Ali *et al.* 1998). In the present study, 12 presynaptic cells having bistratified axons were recorded

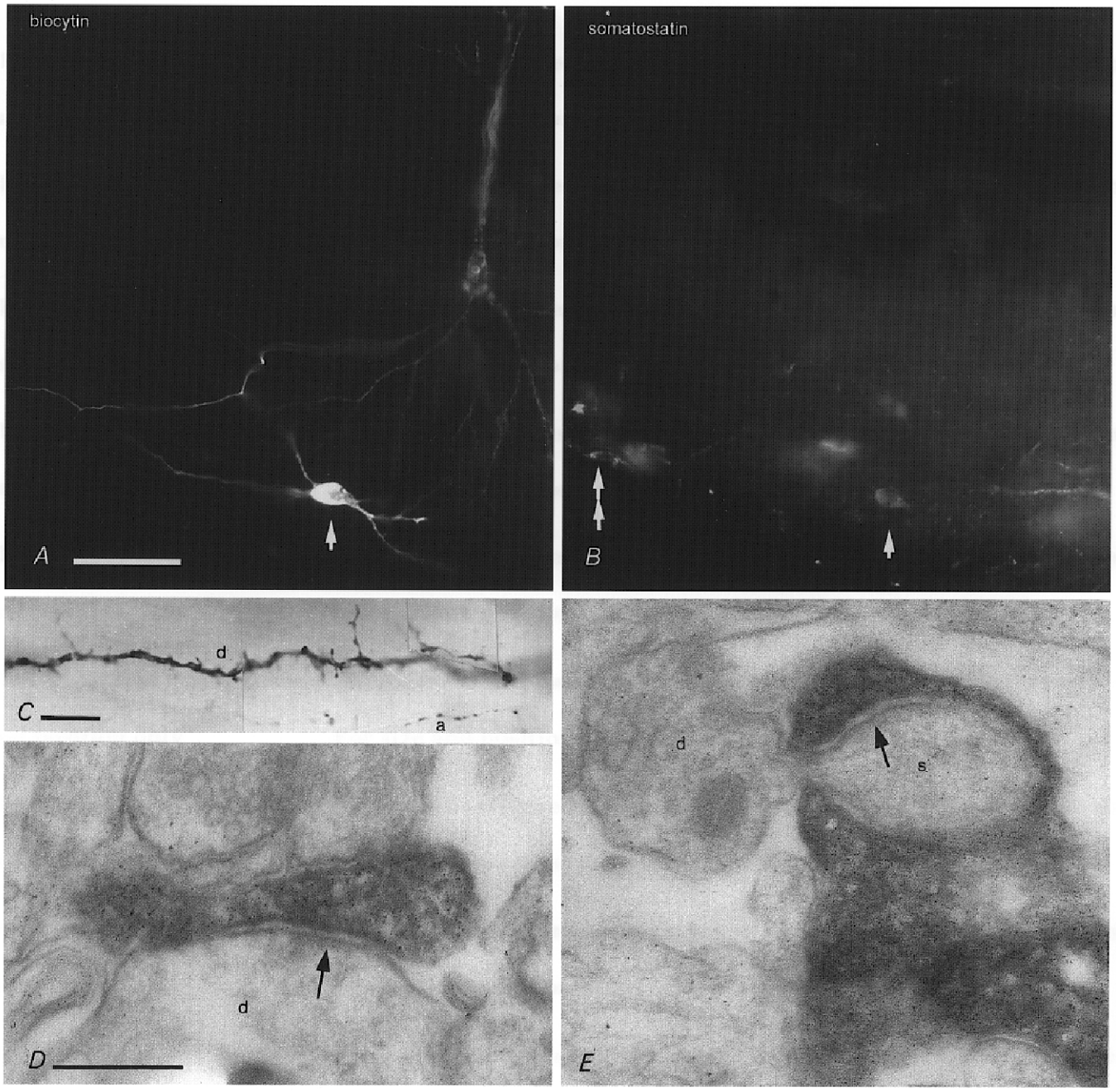


**Figure 3. Somatostatin immunoreactivity and synaptic junctions of O-LM cells**

*A*, micrograph of a biocytin-labelled O-LM cell (arrow, visualised by AMCA-labelled streptavidin, P14) and a pyramidal cell (upper right) that received monosynaptic input from the O-LM cell (see Fig. 1). *B*, the O-LM cell is immunopositive for somatostatin (arrow) as shown by indirect FITC immunofluorescence. Other cells in the same layer (e.g. double arrow) are also immunoreactive. *C*, the dendrites (d) of O-LM cells emit numerous spines and appendages, and the cells often have local axon collaterals (a) in the dendritic field (P14). *D* and *E*, electron micrographs of biocytin-filled boutons of another O-LM cell making synapses (arrows) with a dendritic shaft (d in *D*) or a spine (s) in stratum lacunosum-moleculare (P14). The spine emerging from a small dendrite (d in *E*) is completely surrounded by the bouton, which made a very extensive synaptic specialization as detected in serial sections. Calibration bars: *A* and *B*, same magnification, 50 $\mu$m; *C*, 10 $\mu$m; *D* and *E*, same magnification, 0·2 $\mu$m.

(Table 1). In one case, only the axon was recovered; four cells had multipolar soma and dendrites oriented parallel with the pyramidal apical dendrites as described earlier. However, seven cells had somato-dendritic domains confined to stratum oriens and alveus and oriented parallel with the pyramidal layer (Figs 4 and 5). To our knowledge, such cells with bistratified axons have not been reported earlier. The main axons emitted branches close to their origin, and some branches crossed the pyramidal layer and branched profusely in str. radiatum and oriens. Some axon collaterals of BiCs reached str. lacunosum, but usually turned back into str. radiatum (Fig. 4*A*). Thus, in all seven cases, the axons of BiCs did not innervate str. lacunosum-moleculare, the target domain of O-LM cells. Because of the similarity in somato-dendritic characteristics, in analogy to the name 'O-LM cell', we will refer to cells with bistratified axons and horizontal somato-dendritic domains in str. oriens as O-bistratified cells (O-BiCs). The dendritic innervation is illustrated by the reconstruction of a pair of synaptically coupled cells in Fig. 4*A*. The O-BiC innervated a large border pyramidal cell and 10 light microscopically identified apparent contact sites were found (e.g. Fig. 5*F*), all but one of them provided by a second order axon collateral. The putative contact sites (Figs 4*B* and 5*F*) formed two groups, and involved the main apical dendrite as well as secondary dendritic branches. We analysed 16 and 17 efferent synapses, respectively, from random electron microscopic samples, including all layers, of two cells (Table 2). The overwhelming majority of post-synaptic targets were dendritic shafts (Fig. 5*G* and *H*) and less frequently spines (Fig. 5*I*) and only rarely cell bodies. A few of the dendritic shafts were clearly the main apical dendrites (Fig. 5*H*), but the majority were thin dendritic branches. One neurone with characteristics resembling O-BiCs has been recorded in the CA1 area and labelled *in vivo* and named 'trilaminar interneurone' (Sik *et al.* 1995). The post-synaptic targets of this cell were not evaluated quantitatively.

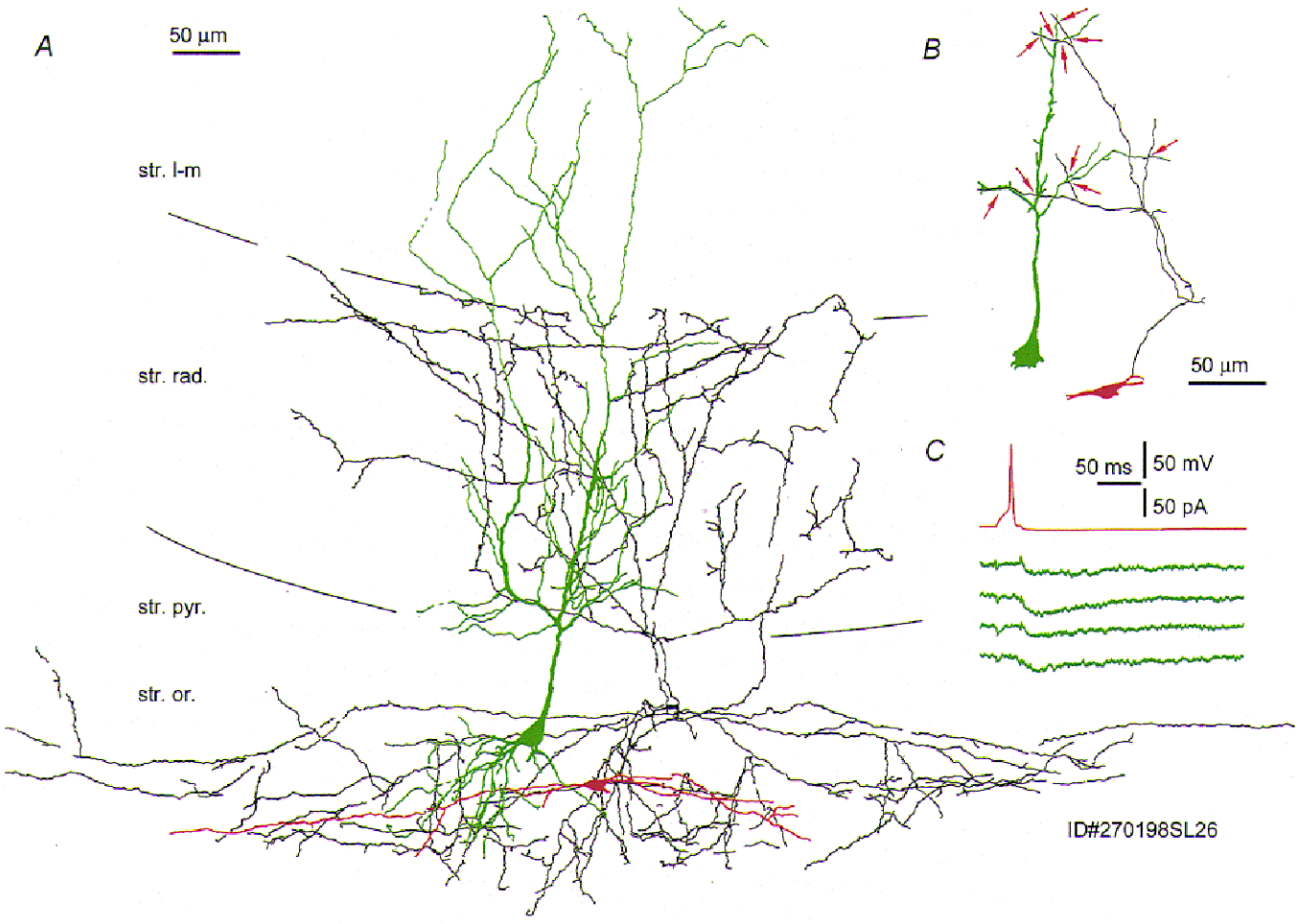


**Figure 4. Reconstruction and synaptic effect of a somatostatin-immunopositive O-BiC on a pyramidal cell at P15 (see also Fig. 5)**

*A*, the axon (black) of the interneurone (soma and dendrites in red) is largely restricted to str. oriens and radiatum and overlaps the dendritic tree of the postsynaptic pyramidal cell (green). Note the sparing by the axon of str. pyramidale, and the dendritic tree restricted to str. oriens. *B*, close appositions (red arrows) of the interneurone axon and the pyramidal dendritic tree. All but one of the appositions are provided by one main axon collateral. *C*, single action potentials in the interneurone evoked slow uIPSCs (single sweeps ) in the postsynaptic pyramidal cell.

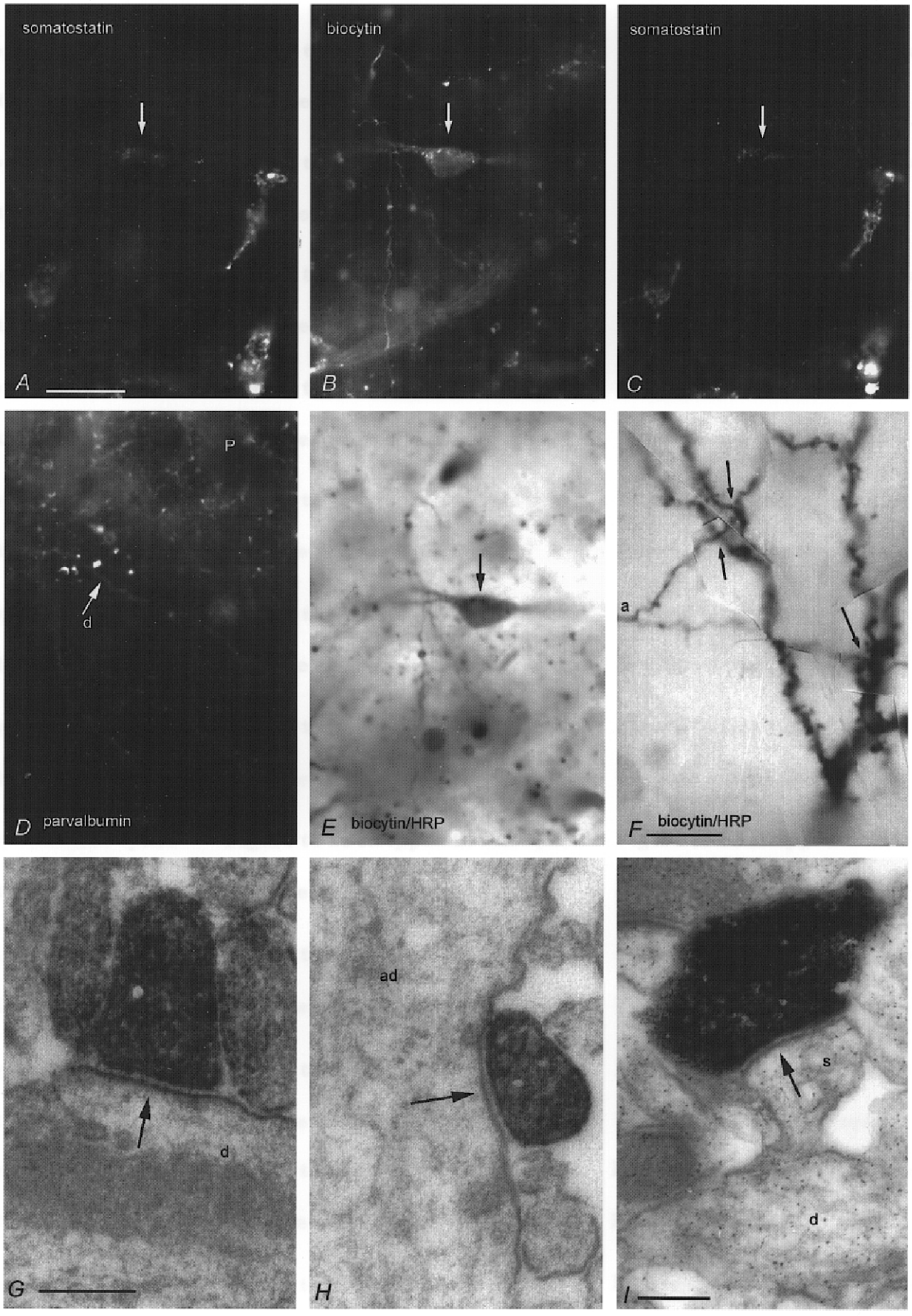


Figure 5. For legend see facing page

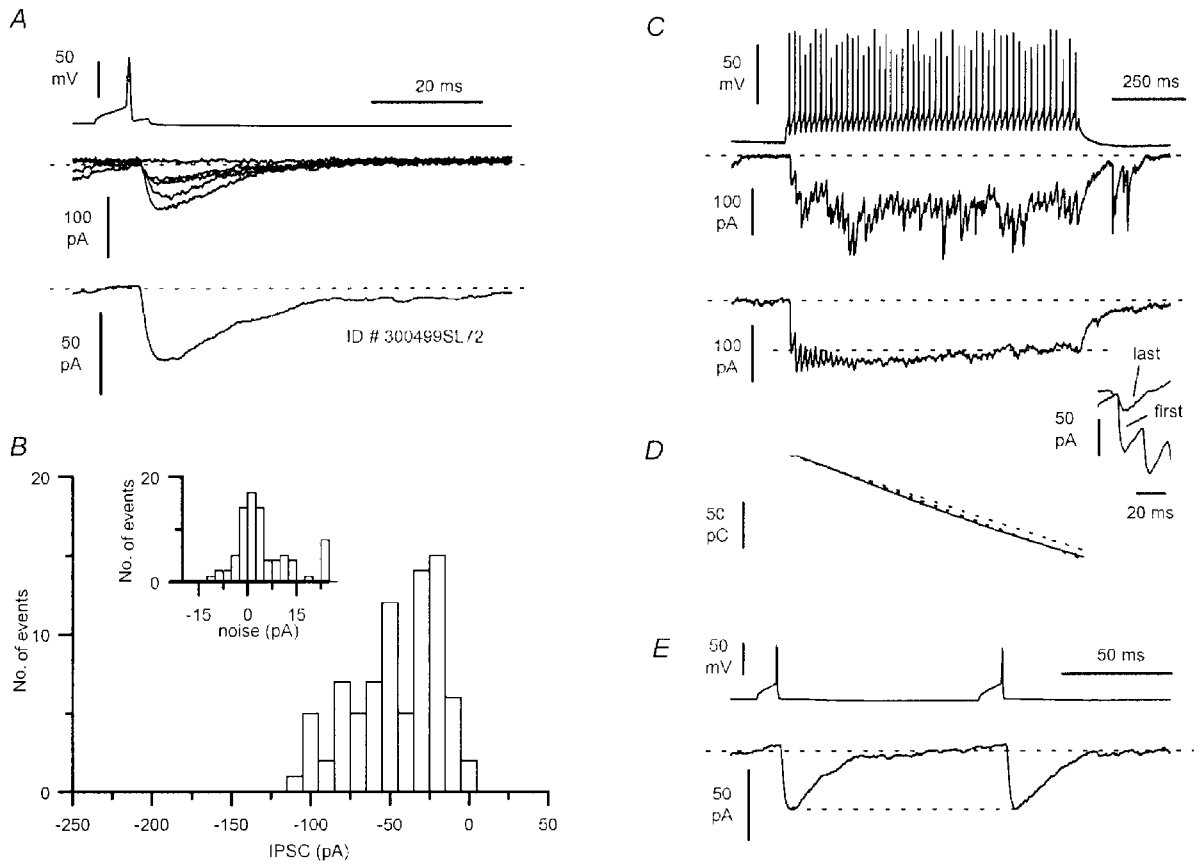


**Figure 6. Postsynaptic effect evoked by a somatostatin-immunopositive O-Bi interneurone**

*A*, postsynaptic IPSCs (single sweeps and average of 81 traces) evoked by single action potentials (P15 animal). *B*, IPSC amplitude and noise (inset) distributions calculated from 81 events. *C*, postsynaptic response to a long train of action potentials evoked by a 200 pA amplitude, 1 s duration current step; single sweep (top) and average of 42 traces are shown. The dashed lines mark the baseline current level and the amplitude of the first IPSC generated by the spike train. The inset on the right compares the IPSCs triggered by the first and the last action potentials in the train after offsetting their respective baselines. *D*, charge transfer during the train of action potentials calculated as the integral of the average summated IPSC (continuous line). Notice the nearly constant slope throughout the time window. Linear fits to the first 100 (top dashed line) and last 500 ms (bottom dashed line) of the charge transfer demonstrate very similar charge transfer throughout the response. *E*, paired action potentials at 100 ms interspike intervals evoked IPSCs of very similar amplitude (average of 81 sweeps).

It remains to be tested if the O-BiCs reported here and the 'trilaminar interneurones' comprise the same class of cells. Similar cells have been described as expressing high levels of the m2 type muscarinic receptor both in their axonal and somato-dendritic domains (Hajos *et al.* 1998). We prefer to use the name O-BiC in order to characterise the main synaptic target domain as determined by electron microscopy. In order to test axonal branches within the pyramidal layer,

**Figure 5. Somatostatin immunoreactivity and synaptic junctions of O-BiCs**

*A* and *C*, an O-BiC (arrow, see also Fig. 4) is immunopositive for somatostatin as shown at two different focal depths by indirect FITC immunofluorescence. Several other cells nearby are also immunopositive. *B* and *E*, micrographs of the same biocytin-labelled cell (arrow), visualised by AMCA-labelled streptavidin (*B*) and peroxidase reaction (*E*). *D*, parvalbumin immunoreactivity was not detected in the cell, but nearby dendrites (d) and varicosities surrounding pyramidal cell bodies (P) showed that immunoreactivity in the area was preserved. *F*, light microscopic photomontage of an axon collateral (a) in close apposition at three sites (arrows) to the postsynaptic pyramidal cell dendrites in str. radiatum (see reconstruction Fig. 4). *G–I*, electron micrographs of biocytin-filled boutons of other O-bistratified cells (P15, *G* and *H*; P14 *I*) are shown to make synapses (arrows) in str. radiatum with a small dendritic shaft (d in *G*), an apical dendrite (ad in *H*) or a spine (s) emerging from a small dendrite (d in *I*). Calibration bars: *A–E*, same magnification, 20 $\mu$m; *F*, 10 $\mu$m; *G* and *H*, same magnification, 0·2 $\mu$m; *I*, 0·2 $\mu$m.

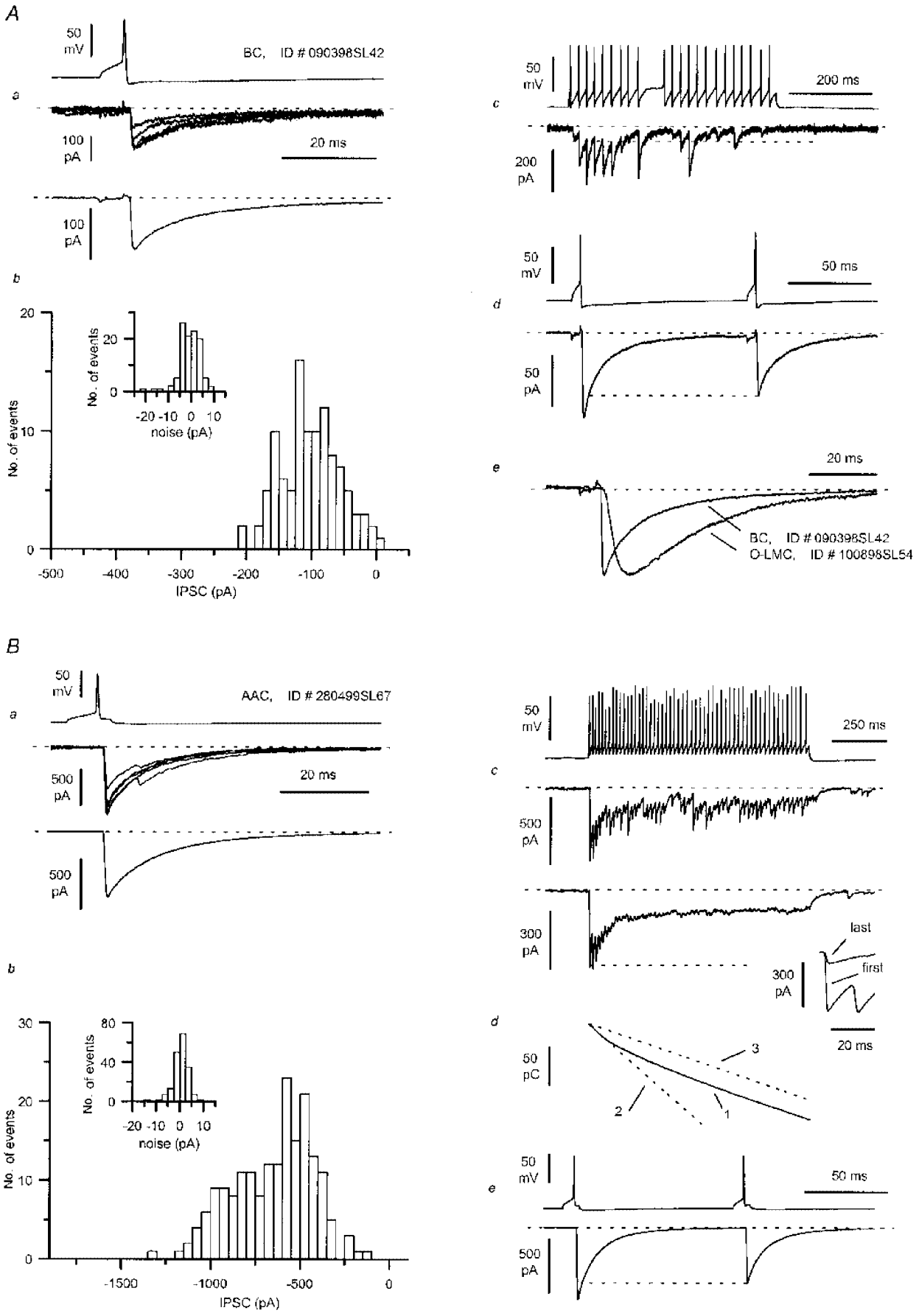


Figure 7. For legend see facing page

one collateral running amongst the pyramidal cells was serially sectioned. Four synapses were tested: in all cases the postsynaptic elements were dendritic shafts, similar to one synapse reported earlier in the pyramidal layer (Sik *et al.* 1995). In summary, the electron microscopic evidence shows the exclusive or, in some cases, predominant dendritic innervation of pyramidal cells by O-BiCs.

Four O-BiCs were tested for somatostatin and three for parvalbumin immunoreactivity. All the cells were immunopositive for somatostatin (Table 1, Fig. 5), but only one for parvalbumin. Parvalbumin immunoreactivity, corresponding to a soluble cytoplasmic protein, is more difficult to detect following whole cell recording than somatostatin immunoreactivity, which is mostly localised to the Golgi apparatus. The physiological properties of the parvalbumin-positive cell were not obviously different from the others. Similar horizontal parvalbumin-positive cells were frequently seen in the str. oriens/alveus region. One of two radially oriented bistratified cells tested was also somatostatin positive. If O-BiCs are somatostatin positive, and comprise a significant population of interneurones, then somatostatin-immunopositive terminals are expected to be present in str. radiatum in appreciable numbers. Therefore, we examined both developing (P13) and adult hippocampus for immunofluorescent labelling for somatostatin. Throughout the CA1 and CA3 regions a fine network of varicose fibres was present in str. radiatum (not shown). The density of varicosities, however, was much lower than in str. lacunosum-moleculare.

The parameters of postsynaptic responses evoked by BiCs were more variable than those of O-LM cells, which is probably related to the variability in the number and placement of synaptic junctions. As clear from previously published examples (Buhl *et al.* 1994; Sik *et al.* 1995; Ali *et al.* 1998), and also found for the BiCs here, individual axonal trees can differ greatly in the radial extent of their laminar distribution. Therefore, the axons of individual BiCs may cover electrotonically extended and variable parts of pyramidal cell dendritic trees. For example, the 10 potential synaptic sites in the reconstructed pair (Fig. 4*B*) were in groups at presumably different electrotonic distances from the soma and resulted in relatively slow uIPSCs (rise time, 2·5 ms; $\tau$, 17·2 ms). The postsynaptic effect of another O-BiC is shown in Fig. 6. Apparent response failures are clearly visible in the recordings (Fig. 6*A*) and in the peak amplitude histogram (Fig. 6*B*). Similarly to O-LMCs, the postsynaptic current generated in response to a prolonged train of action potentials was sustained, as shown both in single sweeps and in averaged records (Fig. 6*C*). The steady state level of postsynaptic current achieved during the train is probably due to the balanced combination of IPSC summation and IPSC depression. Indeed, when the IPSCs triggered by the first and last trains of the pulse were compared, the latter were clearly depressed. Nevertheless, O-BiCs can apparently maintain a constant steady state level of postsynaptic charge flow throughout a prolonged action potential train (Fig. 6*D*), which is in contrast to the effect of BCs and AACs (see below). The response to a pair of action potentials at 10 Hz frequency did not display significant paired-pulse modulation, similar to the responses of O-LMCs (cf. Figs 1*D* and 6*D*).

### Basket cells

Nine basket cells were recorded in str. oriens/alveus (Table 1, Figs 7–11). The cells were identified on the basis of their densest axon centred on the pyramidal layer. In addition they innervated neighbouring areas of str. oriens and

**Figure 7. Properties of the connections between basket (*A*) or axo-axonic cells (*B*) and pyramidal neurones**

*Aa*, single action potentials evoked in a BC (see also Fig. 8*E* and *F*) of a P14 rat are followed by uIPSCs in the postsynaptic neurone (single sweeps and average from $n = 86$ traces). *Ab*, amplitude distribution of the uIPSCs ($n = 107$) and the recording noise (inset). *Ac*, firing pattern and postsynaptic effect during a long train of action potentials evoked by depolarising current (200 pA amplitude 500 ms duration). Note the lack of action potential accommodation and the abrupt period of silence during the train. There is a decline in IPSC amplitude during the train with apparent response failures. The dashed lines mark the baseline current level and the peak of the first IPSC of the train. *Ad*, paired-pulse depression is elicited by two action potentials separated by 100 ms. *Ae*, comparison of the kinetics of the averaged IPSC recorded from the O-LM cell connection shown in Fig. 1, and the one shown in *Aa*. The IPSCs were scaled to the same peak amplitude and superimposed. Note the much longer time to peak of the IPSC evoked by the O-LM cell in comparison with that of the basket cell. *Ba*, unitary events recorded from a pyramidal cell following single action potentials evoked in an AAC (single sweeps and average of 187 traces). *Bb*, peak amplitude distribution of the uIPSC and noise (inset) of the same connection ($n = 187$ records). *Bc*, summated IPSCs evoked by a long train of action potentials, triggered by a 200 pA amplitude, 1 s duration current step; a single sweep (top) and the average of 32 traces are shown. Dashed lines mark the baseline current level and the peak amplitude of the first IPSC. The average IPSCs evoked by the first and last action potentials of the train are compared in the inset on the right after aligning their offset. *Bd*, charge transfer calculated from the average summated IPSC (trace 1). Notice the different slope during the first 100 and last 500 ms of the spike train. Linear fits of these two time windows are clearly divergent (dashed lines 2 and 3, respectively, line 3 shifted to IPSC onset). *Be*, depression of the second response was evoked by two action potentials at 100 ms interspike interval.

radiatum to a differing extent (Figs 9*C* and 11*C*). Basket cells are defined quantitatively by their postsynaptic target being the soma and proximal dendrites of pyramidal cells (Table 2, Fig. 8*E* and *F*). Furthermore, basket cells are heterogeneous according to their neurochemical properties (Freund & Buzsaki, 1996), as expressing either parvalbumin (Kawaguchi *et al.* 1987; Sik *et al.* 1995) or cholecystokinin (CCK) and vasoactive intestinal polypeptide (Freund & Buzsaki, 1996). Therefore, we tested some of the recorded cells immunocytochemically (Table 1). One out of four tested cells was immunopositive (Fig. 10) for the pro-CCK polypeptide (Morino *et al.* 1994), as were scattered cells in all layers, particularly at the border of str. radiatum and lacunosum-moleculare. Most pyramidal cells were also immunopositive (Morino *et al.* 1994) in a perinuclear pattern corresponding to the Golgi apparatus (Fig. 10), but the

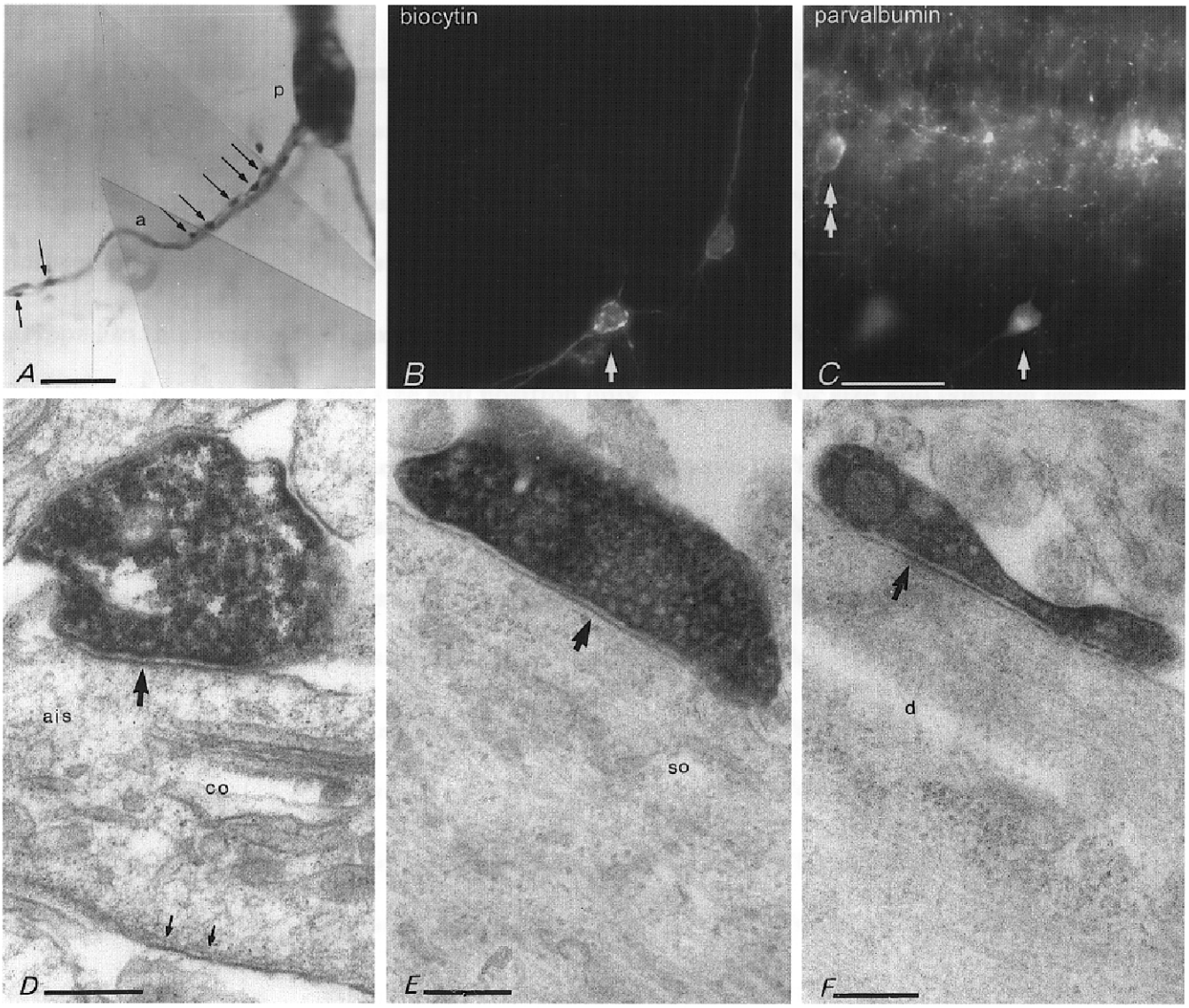


**Figure 8. Perisomatic innervation of pyramidal cells by axo-axonic and basket cells**

*A*, an axo-axonic cell (P13) innervates the axon initial segment (a) of a pyramidal cell (p) at two distinct regions via two axon collaterals providing at least seven boutons (arrows). *B* and *C*, parvalbumin immunoreactivity in another axo-axonic cell (arrows, P14) which evoked a postsynaptic response in a nearby pyramidal cell (to the right in *B*). Another neurone in the pyramidal cell layer (double arrow) and boutons surrounding pyramidal cells are also parvalbumin immunopositive. *D*, electron micrograph of the biocytin-filled bouton of the axo-axonic cell, shown in *B* and *C*, making a type II synapse (upper arrow) with the axon initial segment (ais) of a pyramidal cell. The axon initial segment is identified by the presence of a cisternal organelle (co) and the electron opaque membrane undercoating (small arrows at bottom). *E* and *F*, electron micrographs of biocytin-filled boutons of a basket cell (P14) which was shown to evoke fast uIPSCs in a pyramidal cell (see Fig. 7*A*). The boutons make synapses (arrows) with a pyramidal cell soma (so) or with a large dendritic shaft (d) in stratum pyramidale. Calibration bars: *A*, 10 $\mu$m; *B* and *C*, same magnification, 50 $\mu$m; *D*–*F*, 0·2 $\mu$m.

somatostatin immunoreactive neurones were immuno-negative for pro-CCK. The somato-dendritic axis of the basket cell was oriented parallel to str. pyramidale (Fig. 9*C*), similar to O-LM cells and to a basket cell illustrated by Ramon y Cajal (1893, his Fig. 8, cell b) and Lacaille *et al.* (1987), and also described by McBain *et al.* (1994).

The firing pattern of basket cells is quite different from that of O-LM cells and resembles the firing pattern described for 'fast spiking' hippocampal cells (Kawaguchi *et al.* 1987; Ali *et al.* 1998), as lacking spike frequency accommodation and in some cases having sudden periods of silence during a prolonged current step (e.g. Fig. 7*Ac*). Basket cell-evoked

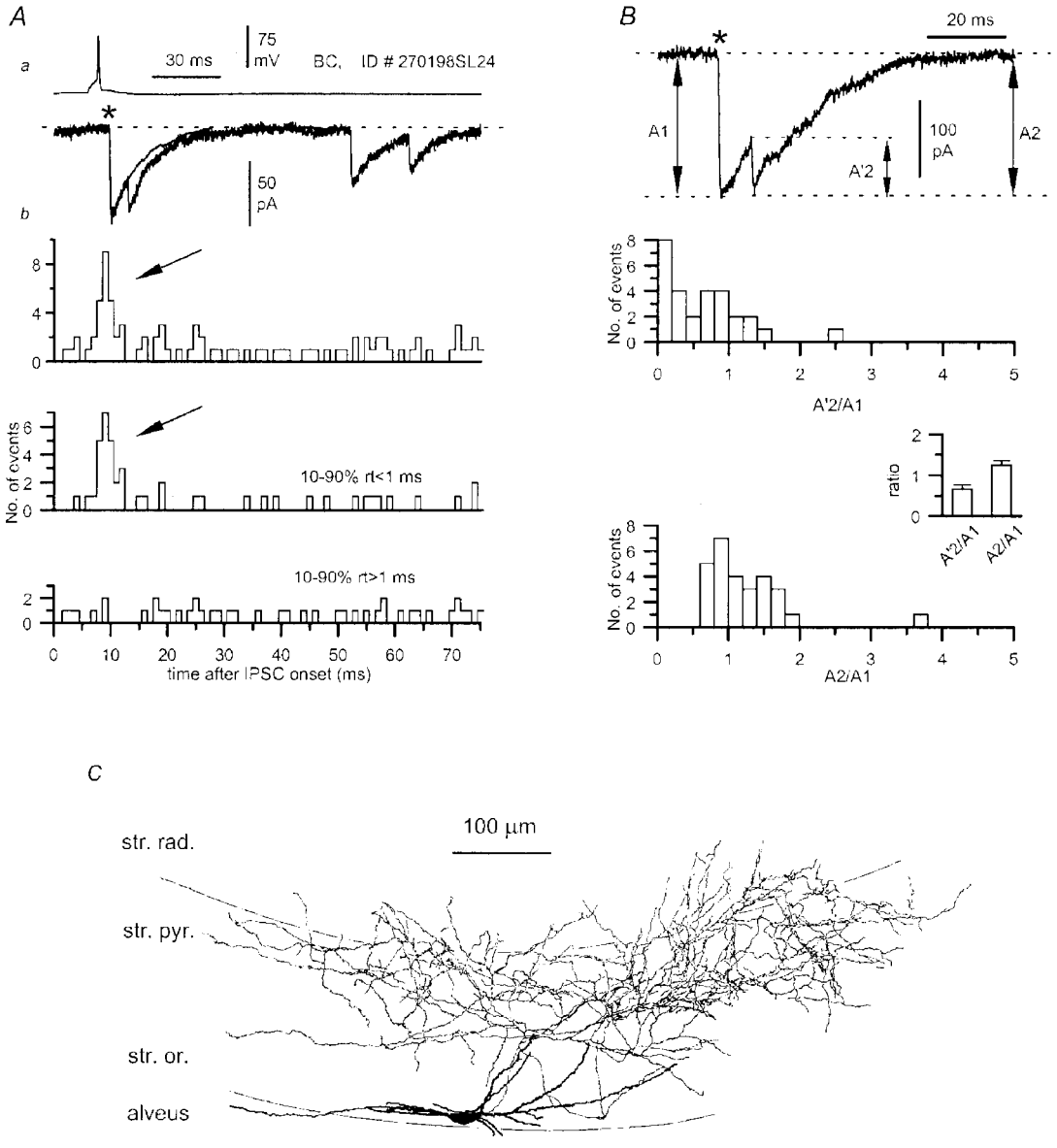


**Figure 9. Multiphasic uIPSC evoked by a CCK-immunopositive basket cell (see also Fig. 10) in a pyramidal cell at P15**

*Aa*, a single action potential generated 'complex' uIPSC is compared to the average kinetics of monophasic responses from the same connection. *Ab*, the distribution of secondary events following the onset of the uIPSC (0, as asterisk in *a*) is shown for all secondary events (top plot) and for events with fast (< 1 ms, middle plot) or slow (> 1 ms, bottom plot) rise times. Note that fast rising secondary events are clustered immediately following the uIPSC (arrows). *B*, amplitude ratios of the asynchronous events. Amplitude ratios were calculated either using the amplitude of the secondary events measured from their onset (A′2) or from the baseline (A2). The distribution for the A′2/A1 ratio and the mean ratio (inset) show that the secondary events had a smaller amplitude than the first ones. The distribution for the A2/A1 ratio and the corresponding mean ratio (inset) show that the absolute peak amplitude levels of first and secondary events were similar. *C*, reconstruction of the presynaptic basket cell of this pair, identified on the basis of the dense innervation of str. pyramidale. The dendrites are restricted to str. oriens/alveus and oriented mainly parallel with the layers.

uIPSCs in pyramidal cells ($n = 9$) were of variable amplitude and kinetics. In some cases, apparent response failures were present, even though their frequency was very low (e.g. Fig. 7*A*, 4% of $n = 107$). In three connections, failures could not be detected. A paired-pulse protocol revealed that at a 100 ms interpulse interval significant depression (37%) was present (Fig. 7*Ad*, see in more detail later). Repetitive firing of basket cells evoked by a long depolarizing current pulse led to an initial summation of IPSCs followed by a sudden decrease in response amplitude, quite different from the response recorded in O-LM and O-BiC interneurones (cf. Fig. 7*Ac vs.* Figs 1*C* and 6*C*). The kinetics of the IPSC were different from those generated by O-LM cells (Fig. 7*Ae*).

Examination of the uIPSCs generated by the CCK-positive and two additional basket cells revealed the presence of 'complex' IPSCs (Figs 9 and 11). Indeed, synaptic activity following the first response was not distributed in time as expected for randomly generated independent events (Figs 9*A* and 11*A*). The probability of the occurrence of secondary events with certain rise time or amplitude (Figs 9*A* and 11*A*) was much higher than expected from background random events, for about 5–10 ms (Figs 9*Ab* and 11*Ab*, arrows) after the onset of the uIPSC. The difference was highly significant. For example, according to Poisson distribution, based on a mean obtained from the frequency of background events (see Methods), the probability of having the observed seven events by chance in the bin 8–9 ms (Fig. 9*Ab*) would be $P < 10^{-7}$. Possible explanations for the high frequency of IPSCs for ~10 ms after the basket cell spike might include the occurrence of multivesicular neurotransmitter release, rebound spikes in other GABAergic cells innervated by the basket cell, or the coupling of several GABAergic cells through gap junctions (Kosaka & Hama, 1985). Secondary events recorded from one pair (Fig. 9*B*) in the 0–20 ms time window were, on the average, smaller than the first one when measured from their onset (A2′/A1 = 0·66). Also, in the same pair, the amplitude of these secondary events measured from the baseline was similar (A2/A1 = 1·25) to the event caused by the first release (Fig. 9*B*). Finally, the kinetics of these secondary events were very similar to those of the uIPSC (rise time < 1 ms). Although all these observations are consistent with the possibility of multivesicular release, the analysis of 'complex' IPSCs recorded in the two additional pairs suggested the alternative hypothesis of electrotonic or other forms of coupling between different presynaptic cells. It is known that interneurone time constants are much shorter than those of pyramidal cells, lending further credence to this possibility. Indeed, in one pair (Fig. 11*A*), secondary events clustering after the first IPSC were of different and relatively large amplitude (> 250 pA) when compared to the first IPSC. The ratio of the amplitudes of secondary to primary events, in the 0–10 ms time window measured from the onset or baseline, were A2′/A1 = 57·1 and A2/A1 = 55·9, respectively (Fig. 11*B*). Furthermore, when the postsynaptic effect of a third basket cell generating 'complex' IPSCs was tested in two postsynaptic pyramidal neurones, 'complex' IPSCs could be recorded only from one of the two targets (Fig. 11*D–F*). This result could

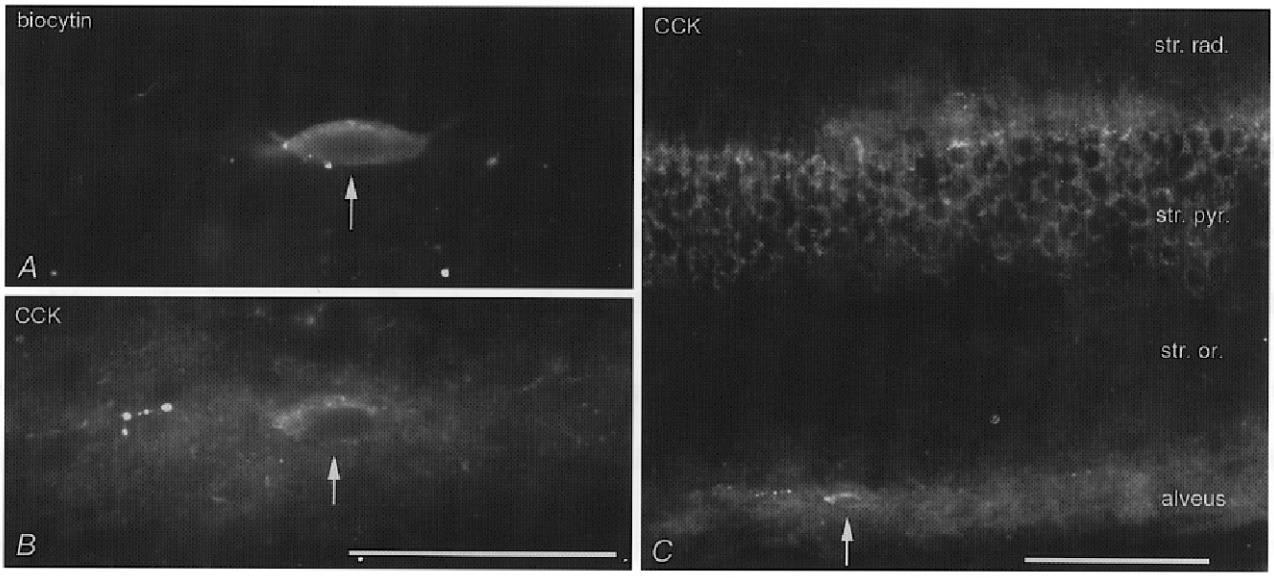


**Figure 10. Pro-CCK immunoreactivity in a basket cell having a cell body in the alveus and dendrites restricted to stratum oriens (see also Fig. 9)**

*A*, micrograph of the biocytin-labelled cell (arrow, visualised by AMCA-labelled streptavidin). *B*, the cell is immunopositive for pro-CCK in a perinuclear band corresponding to the Golgi apparatus, as shown by indirect immunofluorescence (Cy3). *C*, other cells in the same layer are immunonegative, but there is a band of immunoreactive processes in the alveus and lower str. oriens. All pyramidal cells show a perinuclear labelling corresponding to the Golgi apparatus. Calibration bars: *A* and *B*, same magnification, 50 $\mu$m; *C*, 100 $\mu$m.

be more easily explained by some form of coupling between the recorded presynaptic basket cell and an additional interneurone converging onto one of the two target pyramidal cells

### Axo-axonic cells

The postsynaptic effect of six AACs was recorded in seven pyramidal cells (Table 1 and Fig. 7*B*). Axo-axonic cells were identified by their typical axonal arborization and a random electron microscopic sample of postsynaptic targets (Table 2). The latter is necessary because in Wistar rats some GABAergic neurones may target both the axon initial segment and somata as well as dendrites to varying degrees (P. Somogyi & E. Buhl, unpublished observation). All identified synaptic targets ($n = 55$) of six AACs in the present sample were axon initial segments defined on published criteria (Fig. 8*A* and *D*), delineating the interneurones as AACs. The typical initial segment characteristics could not be detected in seven postsynaptic elements to four AACs, probably due to the *in vitro* slice conditions, but this does not exclude the possibility that they were also axons. They were placed in an unidentified category (Table 2).

The kinetics of the uIPSCs were typically fast and the amplitude of the peak response was usually large (Fig. 7*Ba* and *b*) and well separated from the noise. Apparent failures were present in four connections. Presynaptic AACs could sustain regular, non-accommodating spike trains (Fig. 7*Bc*) similarly to BCs. The postsynaptic current generated by a long train of action potentials reached a current level at the end of the train that was much smaller than the peak amplitude of the IPSC originating from the first spike of the train (Fig. 7*Bc*). When plotted as a function of time, the charge transfer during the train of action potentials showed two distinct phases. Linear fitting of the first 100 and last 500 ms of the plot resulted in lines of clearly different slopes (Fig. 7*Bd*). Therefore, it appears that, in contrast to the result obtained for O-LMCs and O-BiCs, summation and depression of the IPSCs generated during the later phase of a repetitive spike train yield a steady state current level that is much smaller than the peak amplitude of the IPSC elicited by the first few action potentials of the train. Finally, when examined with a paired-pulse protocol, at 100 ms interpulse interval, clear depression of the second IPSC was recorded (Fig. 7*Be*, and see below).

### Kinetic properties of uIPSCs

The uIPSCs in CA1 pyramidal cells originate from release sites impinging on distinct somato-dendritic domains as shown here (summarised in Fig. 12*A*). We analysed the relationship between the rise time (10–90 %) and the amplitude of uIPSCs evoked by sets of different types of interneurone; radial- and oriens-BiCs are grouped together. In the case of miniature postsynaptic currents, which are thought to be generated in response to a single quantum of neurotransmitter, correlation between the 10–90 % rise time and amplitude points to dendritic filtering as a factor contributing to the shape of the recorded waveform. In the case of uIPSCs, two additional variables, the number of release sites and asynchronous release (Williams *et al.* 1998) have to be taken into consideration in the interpretation of the plot. The uIPSC rise times were measured for single sweeps from four typical pairs representing the different types of interneurones studied, and also calculated for the averaged unitary events for all the pairs (Fig. 12*B* and *C*). Plots in both cases had a similar 'reverse L' shape, with events likely to originate from proximal and distal sites, rather well separated and located in the arms of the 'reverse L'. The corner region connecting the two arms was mainly occupied by IPSCs generated by BiCs (Fig. 12*B* and *C*). This result is consistent with electrotonic heterogeneity of synaptic sites provided by bistratified cells onto pyramidal cells. That such heterogeneity can occur even in the same unitary connection is shown in individual sweeps in Fig. 12*D*. In this particular case, it was possible to distinguish clearly slow and small-amplitude events (Fig. 12*Da*) and larger and faster currents (Fig. 12*Db*), all having very similar onset following the presynaptic spike. Although variance in quantal size could be responsible for events of different amplitude originating at the same release site, it should not result in a different waveform. The rise time/amplitude plot in this connection clearly reveals the existence of kinetically heterogeneous events with small and large amplitudes (Fig. 12*E*). Despite some scattering of the data points, the correlation between the decay time constant, obtained from monoexponential fits, and the rise time was statistically significant (Fig. 12*F*). This may result from the variable number of active release sites, non-linear dendritic filtering, or the dominance of fast rising and decaying, large amplitude currents in compound events.

Interneurones projecting to the perisomatic area such as AACs and BCs had the largest amplitude and faster events, when compared to BiCs and O-LMCs (Fig. 13). It is noteworthy that within the same cell category the cell to cell variability of BC- and BiC-mediated uIPSCs amplitudes was very high; the coefficient of variation (CV) was 1·55 in both cases, as compared to 0·88 and 1·03 for AACs and O-LMCs. This may be explained by the fact that BCs and BiCs target postsynaptic domains that can be electrotonically heterogeneous, and/or the somatic recording electrode may have also removed some basket cell terminals, thereby increasing the cell to cell variability of the number of release sites. In the case of BCs in particular, it has to be noted that in our sample the BCs eliciting the smaller amplitude IPSCs had a higher proportion of axons in str. oriens and radiatum, probably resulting in a higher proportion of dendritic synaptic sites. Possible cell to cell differences in release probability might also have an effect on the variability of response amplitude. Statistically significant differences in uIPSC amplitudes could only be detected between AACs and O-LMCs ($308 \pm 103$ pA, $n = 7$ *vs.* $26 \pm 10$ pA, $n = 8$, respectively, $P < 0{\cdot}02$).

Variability within the cell groups was generally smaller for either the 10–90 % rise time or decay of the waveforms

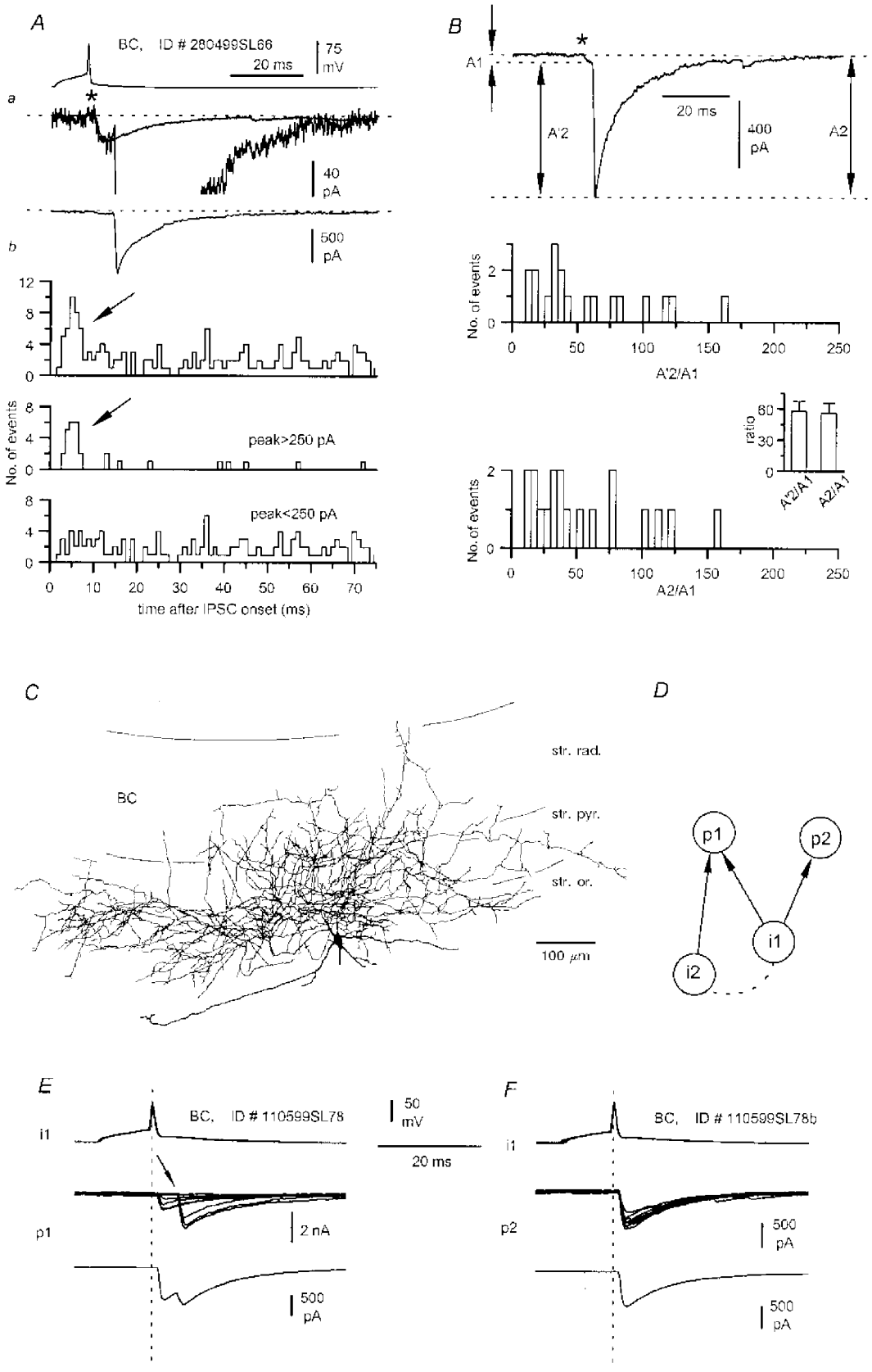


**Figure 11. 'Complex' IPSCs evoked by basket cells may be the result of network interactions**

*Aa*, multiphasic uIPSCs (middle and lower traces, same record at different scales) evoked by a single spike in the presynaptic interneurone (upper trace). Note the small uIPSC preceding the much larger secondary event; the average kinetics for monophasic IPSC from the same connection are superimposed on the single

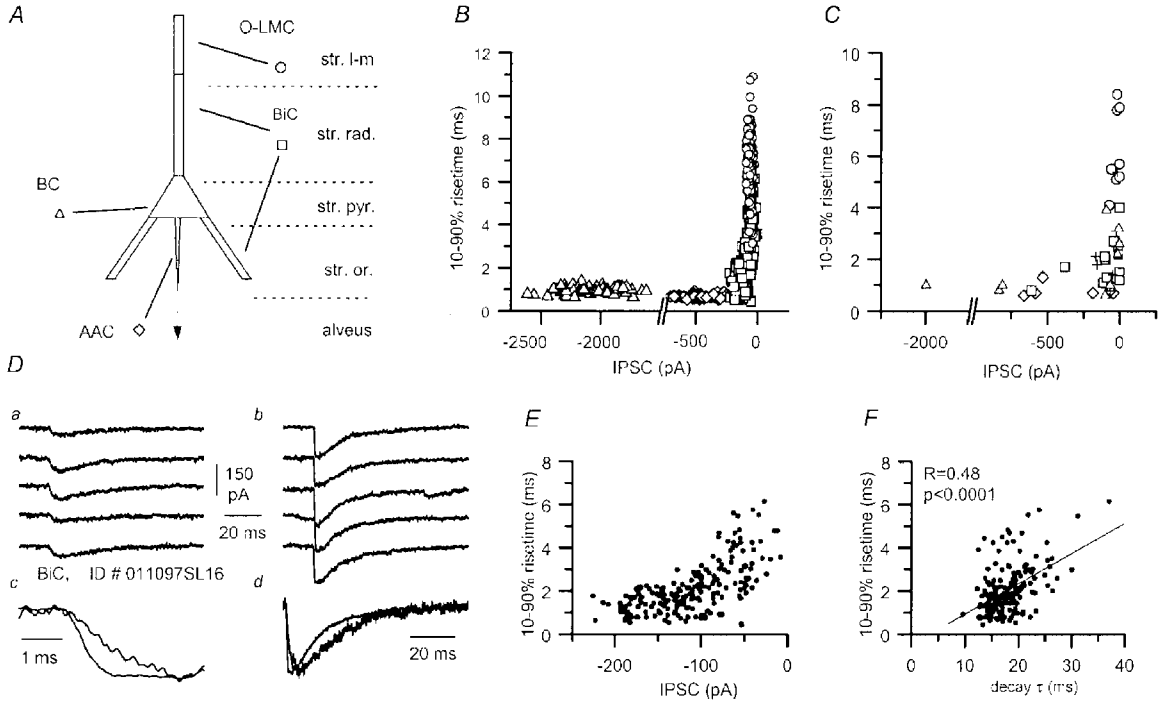


**Figure 12. Presynaptic cell-specific rise times of unitary IPSCs**

*A*, scheme of the different postsynaptic compartments of pyramidal cells and their selective targeting by specific interneurones. *B*, relationship of uIPSC rise time and amplitude. IPSCs (single sweeps) evoked by four distinct interneurones are plotted: an AAC (diamonds), a BC (triangles), a BiC (squares) and an O-LMC (circles). *C*, similar plot obtained from the average unitary IPSC of all connections studied (AAC, $n = 7$; BC, $n = 9$; BiC, $n = 13$; O-LM, $n = 8$). Symbols are as in *A*, and in addition, the effects of unidentified presynaptic interneurones are marked by crosses. The properties of responses evoked by a given cell type tend to differ from all other cell types. *D*, comparison of selected sweeps from a BiC to pyramidal cell connection (P12) showing variability of uIPSC kinetics. Slower and smaller (*a*) as well as faster and larger (*b*) responses were observed. Averages of the 5 traces (*c* and *d*) are shown scaled to the same peak amplitude at two different time scales. *E*, the relationship of IPSC rise time and amplitude for the same BiC to pyramidal cell connection shows a biphasic distribution of IPSCs. *F*, the IPSC decay to rise time relationship of the same responses showed a significant correlation.

(Fig. 13). Consistent with a more heterogeneous electrotonic location of their synaptic sites, BC- (CV = 0·66) and BiC-mediated (CV = 0·43) IPSCs had higher CVs than did those evoked by AACs (CV = 0·30) or O-LMCs (CV = 0·26). Statistically significant differences were found between 10–90% rise times of IPSCs mediated by AACs *vs.* events mediated by BiCs or O-LMCs (0·8 ± 0·1 ms, $n = 7$ for AACs *vs.* 2·0 ± 0·2 ms, $n = 13$ for BiCs, $P < 0{\cdot}01$; and 6·2 ±

sweep. *Ab*, the distribution of secondary events following the onset of the first IPSC (asterisk) is shown for all secondary events (top plot) and for events with large (peak > 250 pA, middle plot) or small (peak < 250 pA, bottom plot) amplitudes. Large secondary events are more frequent immediately following the uIPSC (arrows). *B*, amplitude ratios of the large (> 250 pA) asynchronous events occurring in the 0–10 ms time window. Ratios were calculated either using the amplitude of the secondary events measured from their onset (A′2) or from the baseline (A2). The distribution for the A′2/A1 ratio and the mean ratio (inset) show that the secondary events had a much larger amplitude than the first ones. The distribution for the A2/A1 ratio and the corresponding mean ratio (inset) show that the absolute peak amplitude levels of first and secondary events were very different. *C*, reconstruction of the presynaptic basket cell shown in *A* and *B* and identified on the basis of its postsynaptic target domains (Table 2). Note the relatively wide distribution of the axon to different layers. *D*, schematic diagram of a possible network circuit underlying 'complex' IPSCs. Synaptic connections are indicated by arrows, putative gap junction, or other form of interneuronal interaction by dashed lines. *E* and *F*, postsynaptic effect of a single presynaptic basket cell (i1) onto two distinct pyramidal neurones recorded sequentially (p1 and p2) at P14. Notice that 'complex' IPSCs (single sweeps and average of 22 and 245 traces, respectively) evoked by a single spike can be recorded only from one (p1) of the two postsynaptic pyramidal cells. Vertical dashed lines are shown for reference.

0·6 ms, $n = 8$ for O-LMCs, $P < 10^{-6}$). Also, statistically significant differences were present between the 10–90% rise time of IPSCs mediated by O-LMCs *vs.* BiCs or BCs (6·2 ± 0·6 ms, $n = 8$ *vs.* 2·0 ± 0·2 ms, $n = 13$, $P < 10^{-6}$; and 1·8 ± 0·4 ms, $n = 9$, $P < 10^{-4}$, respectively). In summary, the rise time of uIPSCs evoked by the AACs was consistently fast (<1 ms), some BC- and BiC-mediated events could be similarly fast, but some were slower (>1 ms), and finally, O-LMC-mediated IPSCs were consistently slower (>3 ms), in accordance with what would be expected by an influence of dendritic filtering.

The decay phase of the unitary IPSCs was also variable within the different sets of interneurone types; the CV for AACs was 0·21 ($n = 7$), for BCs 0·28 ($n = 9$), for BiCs 0·25 ($n = 13$) and for O-LMCs 0·23 ($n = 8$). For two O-LMCs exponential functions provided a poor fit of the IPSC decay. Therefore, the manually measured time to 63% of the decay was used in the analysis instead of the decay time constant, $\tau$. In six other cases (2 AACs, 3 BCs and 1 unidentified cell) biexponential functions fitted best the decay kinetics, which were characterised by the weighted average of the two time constants (Fig. 13*D*). In the rest of the recordings monoexponential fits were used. Striking differences in the decay, such as those reported by Pearce *et al.* (1995) and Banks *et al.* (1998) for IPSCs evoked by extracellular stimulation, were not observed. However, the overall mean decay time course of the connections had a trend giving higher values for more distally targeting presynaptic interneurones. Accordingly, AACs generated faster decaying events as compared to BiCs or O-LMCs (11·2 ± 0·9 ms, $n = 7$, *vs.* 16·1 ± 1·1 ms, $n = 13$, for BiCs, $P < 0{\cdot}01$; and 20·8 ± 1·7 ms $n = 8$, for O-LMCs, $P < 10^{-3}$). On the other

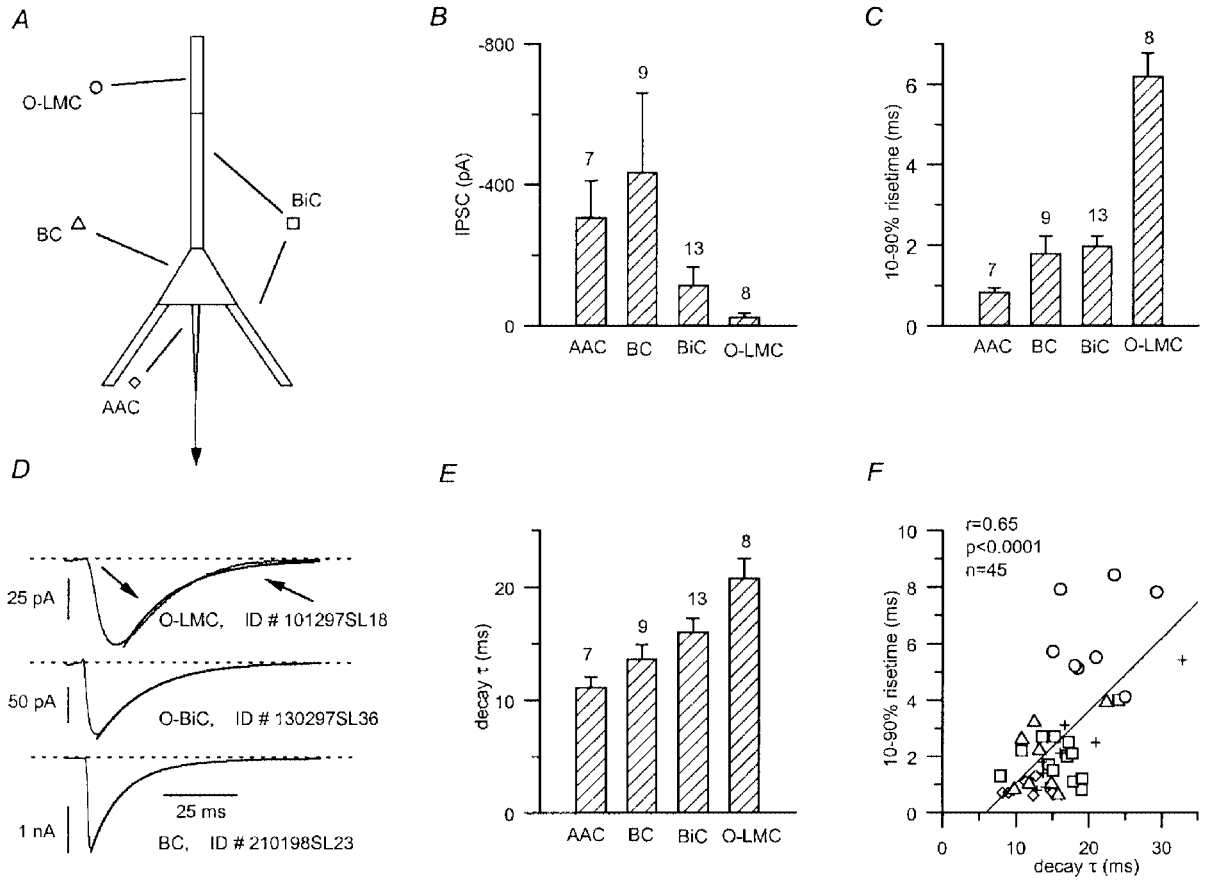


**Figure 13. Kinetic properties of uIPSCs evoked by different cell types**

*A*, schematic diagram of a pyramidal cell indicating the segregated postsynaptic domains for distinct presynaptic interneurones. *B*, comparison of the amplitudes of uIPSCs evoked by different interneurones; note the larger amplitude of perisomatically generated IPSCs (AAC and BC). Numbers of cells analysed are shown above bars. *C*, rise times (10–90%) of uIPSCs show a trend towards higher values with increasing electrotonic distance of the postsynaptic domain from the somatic recording site. *D*, approximating the decay phase of uIPSCs with exponential functions could result in a poor monoexponential fit (upper trace, arrows, O-LM cell, P17), a good monoexponential fit (middle trace, O-BiC, P15), or a good biexponential fit (bottom panel, BC, P16). *E*, the difference in the decay ($\tau$, time to 63% of decay, or weighted average of the two $\tau$) of IPSCs, generated by different classes of presynaptic interneurones, reached statistical significance in several comparisons (see text). *F*, relationship between the rise time and decay of all recorded uIPSCs (for symbols see *A*). A significant positive correlation indicates electrotonic filtering as a contributing factor to heterogeneity.

hand, O-LMCs generated slower decaying events than all other cell types (20·8 ± 1·7 ms, $n = 8$ for O-LMCs, *vs.* 13·7 ± 1·3 ms, $n = 9$, for BCs, $P < 0·01$; and 16·1 ± 1·1 ms, $n = 13$, for BiCs, $P < 0·05$). Rise times and decay time constants for the whole set of uIPSCs were significantly correlated (Fig. 13*F*), indicating electrotonic filtering (Spruston *et al.* 1993) as the main determinant of the somatically recorded apparent IPSC kinetics, although other factors, like a possible heterogeneity of $GABA_A$ receptors at specific postsynaptic domains, might also contribute to the observed kinetic differences.

In all cases tested (2 O-LM cells, 2 BiCs and 2 O-BiCs), regardless of the kinetics, the unitary IPSCs were sensitive to blockade by bicuculline (Fig. 14), confirming that the recorded uIPSCs originated from the activation of $GABA_A$ receptors. $GABA_B$ receptor-mediated uIPSCs could not be evaluated under our experimental conditions, because of the presence of caesium and QX-314 inside the recording pipette.

### Short-term plasticity of IPSCs

Following repeated activation, $GABA_A$ receptor-mediated IPSCs were reported to be depressed in the hippocampus and several mechanisms could be involved (Davies *et al.* 1990; Pearce *et al.* 1995). The changes in IPSCs were investigated by paired presynaptic action potentials in 34 connections of the present sample, to test whether the synapses of different cell types responded uniformly. The sample included six AACs, eight BCs, 11 BiCs, six O-LMCs and three unidentified interneurones. We used an interpulse interval of 100 ms (see also Oardouz & Lacaille, 1997) in order to mimic the average firing frequency that has been reported in recordings of str. oriens/alveus interneurones *in vivo* (Csicsvari *et al.* 1999). Under these conditions facilitation, depression or no change of the second IPSC could be observed (Fig. 15*A–C*). However, the kinetics of the second response did not change in comparison with the first one (Fig. 15*A–C*). This result indicates a uniform paired-pulse regulation of all release sites present in any one unitary connection, irrespective of the kinetic differences of single responses, as for instance, in the BiC-evoked response shown in Fig. 12. We did not observe in any tested uIPSC the kinetic change of the second response reported by Pearce *et al.* (1995) for IPSCs evoked by stimulation of str. radiatum. In this overall population of uIPSCs, the degree of short-term depression or facilitation was not linearly correlated with either the 10–90% rise time of the IPSC or its amplitude (Fig. 15*D*). However, the degree of depression was related to the identity of the presynaptic interneurone. On average, interneurones more biased towards targeting the dendritic region tended to have less paired-pulse modulation. The ratio of the second IPSC over the first one was 0·68 ± 0·05 ($n = 6$) for AACs, 0·89 ± 0·13 ($n = 8$) for

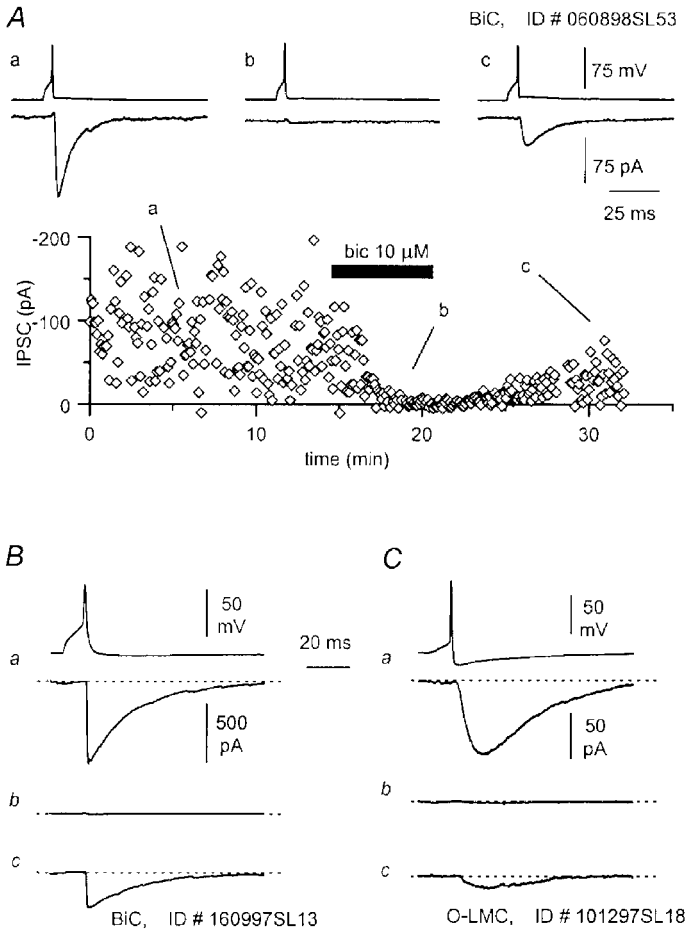


**Figure 14. Unitary IPSCs evoked by different types of interneurones are mediated by $GABA_A$ receptors**

*A*, time course of bicuculline block of a uIPSC evoked by a BiC (P14), and partial recovery of the response during wash-out of the antagonist. Traces show averaged responses in control solution (*a*), during bicuculline superfusion (*b*) and after partial wash-out of the drug (*c*). *B*, the effect of bicuculline on uIPSCs evoked by another BiC (P11) having its cell body located near the pyramidal cell layer (traces as in *A*). *C*, similar effect of bicuculline on a uIPSC evoked by an O-LM cell (P17).

BCs, 1·09 ± 0·18 ($n = 11$) for BiCs and 0·93 ± 0·04 ($n = 6$) for O-LMCs. Variability of the paired-pulse ratio was more pronounced for BCs (CV = 0·41, $n = 8$) and BiCs (CV = 0·55, $n = 11$), whereas AACs (CV = 0·17, $n = 6$) and O-LMCs (CV = 0·09, $n = 6$) were remarkably homogeneous in this respect. A statistically significant difference was found between AACs and O-LMCs ($P < 0·001$).

## DISCUSSION

The results show that: (i) interneurones in str. oriens/alveus having horizontal dendrites include O-LMCs, O-BiCs and BCs with segregated efferent synaptic target domains; (ii) $GABA_A$ receptor-mediated uIPSCs can be generated along the whole somato-dendritic domain and the axon initial segment; (iii) uIPSCs generated by O-LMCs in the most distal pyramidal dendrites in str. lacunosum-moleculare are detectable in the soma; (iv) the somatically recorded kinetics reflected the domain of innervation; and (v) short-term plasticity of IPSCs is characteristic of the presynaptic cell type.

### Interneurones of str. oriens/alveus

The local axonal collaterals of pyramidal cells in CA1 are restricted to str. oriens/alveus. Therefore, interneurones whose dendritic trees are co-aligned with the pyramidal axons are likely to receive their major input from pyramidal cells (Baude *et al.* 1993). This indeed has been demonstrated for the O-LMC (Lacaille *et al.* 1987; Blasco-Ibanez & Freund, 1995; Maccaferri & McBain, 1995; Ali & Thomson 1998), but not yet for O-BiCs and horizontal BCs. Our results raise the possibility that recurrent pyramidal input is channelled to the perisomatic area (BC), the Schaffer collateral, commissural zone (O-BiC) and the entorhinal termination zone (O-LMC) by three distinct sets of interneurones, in addition to radially oriented BCs and BiCs.

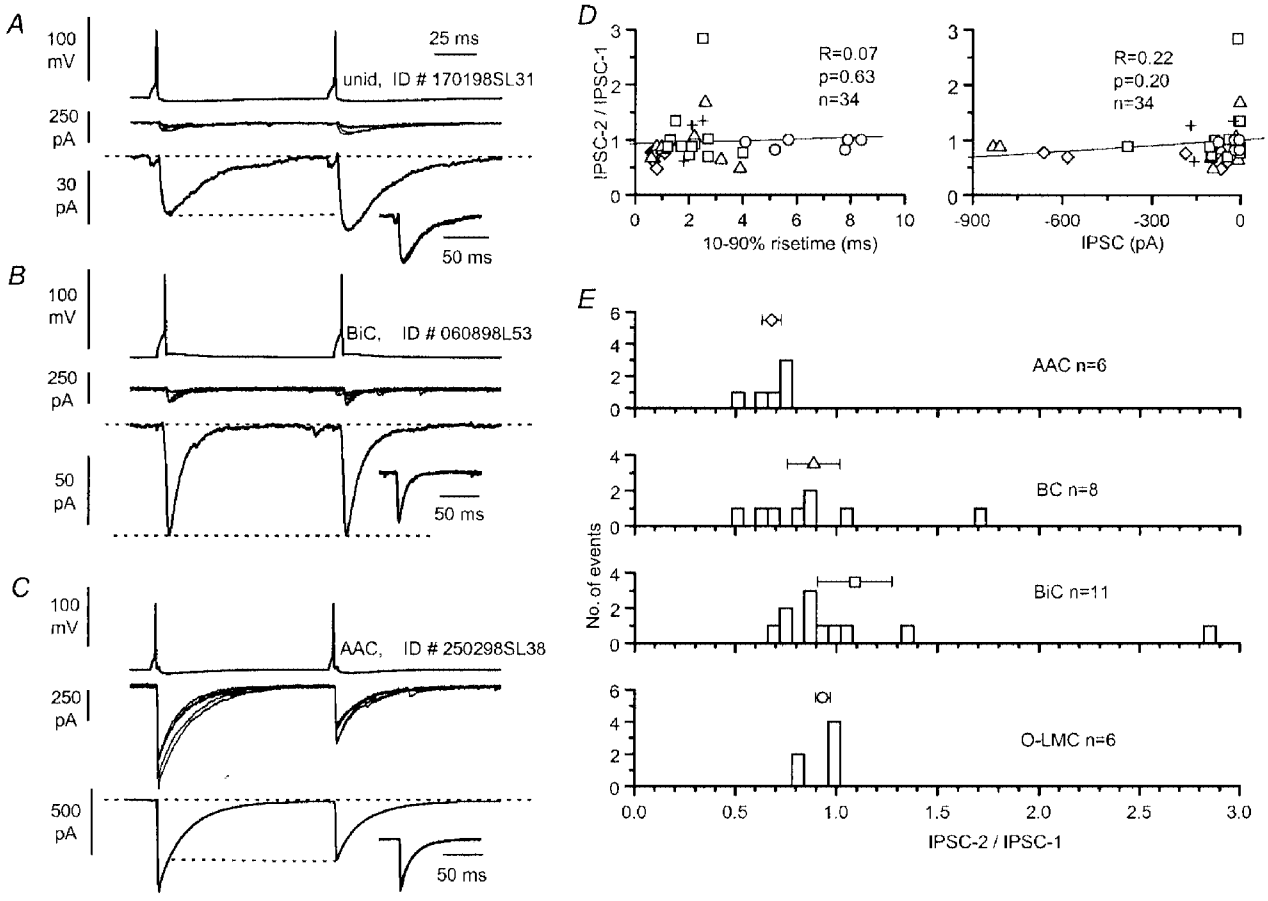


**Figure 15. Heterogeneity and variability in short-term plasticity of different types of unitary connections**

*A–C*, pairs of action potentials at 100 ms interspike interval resulted in either facilitation (*A*, unidentified interneurone, P16), no change (*B*, BiC, P14) or depression (*C*, AAC, P16) of the second postsynaptic response. Superimposed single sweeps (middle traces), displayed at the same scale for comparison, and averages ($n = 50$, 61 and 54 events, respectively) are shown. The insets demonstrate that the kinetics of the two events remained very similar as shown by scaling and superimposition of the pairs of responses. *D*, the degree of paired-pulse change does not appear to correlate with either the rise time (left panel) or the amplitude of uIPSCs (right panel) in the overall population. *E*, the distributions of the amplitude ratio of the second response over the first IPSC and their mean ± S.E.M. (symbols as in Fig. 13) are shown sorted according to the type of the presynaptic interneurone.

We have shown unequivocally that O-LMCs are somatostatin immunoreactive. This is consistent with the orientation of somatostatin-positive cells of str. oriens/alveus and axons in str. lacunosum-moleculare (Naus *et al.* 1988; Baude *et al.* 1993; Katona *et al.* 1999). We have also identified another somatostatin-positive cell type, the O-BiC, which shares its somato-dendritic features with the O-LMCs, but an axonal target domain with radial BiCs. This cell is responsible for somatostatin-immunopositive varicosities in str. radiatum in our study and also reported recently (Katona *et al.* 1999). The functional comparison of BiCs in str. pyramidale and O-BiCs remains to be investigated. *In vivo*, interneurones in str. pyramidale and oriens/alveus discharge differentially in relation to theta and sharp wave population activity (Csicsvari *et al.* 1999), but the firing patterns of the interneurone classes studied here are not known. At the synaptic level, BiCs of str. pyramidale show paired-pulse depression of their CA1 pyramidal input (Ali *et al.* 1998). In contrast, at least one class of 'horizontal' cell, the O-LMC, displays facilitation of its pyramidal cell input (Ali & Thomson, 1998). Horizontally oriented interneurones may constitute a distinct group because their input may originate mostly from local pyramidal cells.

### Kinetic properties of IPSCs evoked by different GABAergic interneurones

The kinetics of unitary IPSCs, as apparent from somatic recordings, was variable and dependent on the synaptic target domain of the presynaptic interneurone, raising the possibility that factors related to target domain specificity such as electrotonic filtering or site-specific subunit composition of $GABA_A$ receptors might contribute to the observed kinetic differences. Unitary IPSCs evoked by O-LMCs ($IPSC_{O\text{-}LM}$) had very slow rise times, but the same postsynaptic pyramidal cells showed spontaneous events with much faster kinetics. Two kinetically and pharmacologically distinct $GABA_A$ receptor-mediated IPSCs have been described (Pearce, 1993). However, we never recorded IPSCs with decay time constants slower than 35 ms (Pearce, 1993; Banks *et al.* 1998). Furthermore, $IPSCs_{O\text{-}LM}$ were usually smaller in amplitude than the unitary events with faster rise time generated by perisomatic targeting interneurones like AACs ($IPSC_{AAC}$) or BCs. This is consistent with a difference in the waveform due to dendritic filtering (Spruston *et al.* 1993; Soltesz *et al.* 1995). We used animals of a postnatal age range overlapping that of Banks *et al.* (1998), and therefore it is unlikely that developmental processes underlie the difference in IPSC kinetics between the two sets of data. A distinct pool of functionally untested cells (Hajos & Mody, 1997) might generate the 'slow' IPSCs (Pearce, 1993).

Identification of our $IPSCs_{AAC/BC}$ with the 'fast' events evoked by stimulation of str. pyramidale (Pearce, 1993) and/or 'fast' spontaneous IPSCs (Banks *et al.* 1998) is more likely. Such events have been suggested to originate on or close to the soma (Soltesz *et al.* 1995). Rise times, decay time constant values and the degree of paired-pulse depression calculated for $IPSCs_{AAC}$ in our study are in a range similar to the values reported for some of the 'fast' IPSCs (Pearce *et al.* 1995; Banks *et al.* 1998). However, uIPSCs with fast rise time ($<1$ ms) and fast decay time constants ($<10$ ms) could be evoked also by some BCs and BiCs. In the latter cell groups, some of the other unitary connections, presumably located on electrotonically more distant sites, shifted the average towards higher values and increased the CV. Nevertheless, AACs and BCs are the most likely source of furosemide-sensitive IPSCs (Banks *et al.* 1998), suggesting the presence of $\alpha 4$ subunit containing postsynaptic $GABA_A$ receptor. The location of the $\alpha 4$ subunit on pyramidal cells is not known. The distribution of $\alpha 1$ and $\alpha 2$ receptor subunits is partially different, the $\alpha 2$ subunit being more frequent in the synapses of AACs in comparison with those of BCs (see Somogyi *et al.* 1998). In addition, other factors, like the phosphorylation state of synaptic receptors (Jones & Westbrook, 1997; Poisbeau *et al.* 1999), or the mechanisms of transmitter release (Williams *et al.* 1998), can affect the kinetics of IPSCs. Notwithstanding the numerous factors discussed above, in our recordings the most parsimonious explanation for the location-dependent kinetic differences in uIPSCs is electrotonic filtering and/or the lack of voltage clamp at the more distal locations (Spruston *et al.* 1993). Supporting this conclusion, rise time values and decay time constants for the total sample of uIPSCs were indeed significantly correlated. However, our data do not exclude the possibility that differences in channel kinetics might also contribute to location-dependent kinetic variation of uIPSCs, if the composition or state of synaptic receptors varies along the surface of pyramidal cells.

A precise determination of the real, 'on site' synaptic current kinetics in dendrites is still lacking. Even recordings of uIPSCs at different locations along the dendritic tree of pyramidal cells would present difficulties. First, recordings in the distal dendrites are usually associated with a very high series resistance. Second, uIPSCs at distal locations are likely to be generated by release at multiple synaptic sites located on different dendritic branches (see e.g. Fig. 2). Thus, even a recording pipette positioned close to one of the contact sites would be at variable distance from the others, which together would generate a response recorded under the influence of dendritic filtering and uneven voltage clamp.

The time course of IPSCs is influenced also by network interactions amongst interneurones. 'Complex', multiphasic responses were evoked in three BC connections, suggesting some form of coupling of several presynaptic interneurones. Fast network mechanisms involving interactions through glutamatergic synapses are very unlikely to be involved because the recordings were performed in the presence of D-AP5 and DNQX to block AMPA and NMDA receptor-mediated excitatory transmission. One possible mechanism could be electrotonic coupling through gap junctions, which was shown to synchronise the firing of cerebellar GABAergic interneurones (Mann-Metzer & Yarom, 1999). It was shown that due to an interaction of the coupling potential with

voltage dependent intrinsic conductances, the window of synchronisation is wider than expected from the duration of the coupling potential and is compatible with the 5–10 ms delay observed here in the hippocampus. Thus, similar interneurones could be rapidly recruited and provide synchronised GABAergic effects onto a given postsynaptic domain. Rebound firing of other interneurones receiving innervation from the presynaptic cell and converging on the same postsynaptic pyramidal cell seems less likely, because rebound spikes usually occur after much longer latencies than 10 ms, at least in pyramidal cells (Cobb *et al.* 1995). Asynchrony of neurotransmitter release among different release sites due to conduction delay along the axon is also unlikely (Williams *et al.* 1998), but the results do not exclude the possibility that mulitvesicular release might occur and contribute to the generation of some multiphasic uIPSCs (Auger *et al.* 1998).

### Short term plasticity

Heterogeneity of paired-pulse depression (Pearce *et al.* 1995) and presynaptic regulation have been reported for IPSCs in pyramidal cells. A clear difference in paired-pulse depression between IPSCs generated by O-LM and AACs has been found here. The cellular and molecular mechanisms that are responsible for these differences are not known. Structural and functional properties of the presynaptic terminals as well as heterogeneity of postsynaptic $GABA_A$ receptors or their regulatory pathways could play a role in determining the degree of short-term plasticity of specific GABAergic connections. Unlike the $IPSC_{O\text{-}LM}$ reported here, the IPSPs generated by neocortical somatostatin-containing neurones were reported to show marked paired-pulse depression (Reyes *et al.* 1998). The reason for this difference is not known. The sample of recorded BiCs showed heterogeneous properties possibly due to the inclusion of several neuronal subtypes. The relative lack of depression of IPSCs generated by O-LMCs is consistent with our suggestion that these cells cannot be the sources of the 'slow' IPSCs (Pearce *et al.* 1995) having the highest level of paired-pulse inhibition. Depression of IPSCs generated by AACs was consistent with their identification with cells producing 'fast' IPSCs (Pearce *et al.* 1995).

Presynaptic cell specific short-term plasticity could be relevant to the particular role of each neuronal class. Inhibition at the axon initial segment and soma may primarily govern the timing of fast action potentials most effectively at low presynaptic firing rates as both their inputs (Ali *et al.* 1998) and their outputs depress. During repetitive, high frequency firing of pyramidal cells, recurrent activation of O-LMCs could lead to a relatively non-decremental charge transfer generated in the distal pyramidal dendrites. During high frequency GABA release, $GABA_B$ receptors may also be activated (Thomson *et al.* 1996; Yanovsky *et al.* 1997). All previously tested uIPSPs were also mediated by $GABA_A$ receptors (Miles & Wong, 1984; Buhl *et al.* 1994), but some classes of GABAergic cell have not been tested for the receptor mechanisms of their postsynaptic effect.

### Possible role of dendritic innervation by O-LM and O-BiCs

A non-decrementing $GABA_A$ receptor activation on the dendrites of pyramidal cells could simply shunt entorhinal or Schaffer collateral EPSPs, respectively, or reduce their effectiveness through dendritic hyperpolarization (Maccaferri & McBain, 1995; Katona *et al.* 1999). Alternatively, it could shunt and limit regenerative postsynaptic responses and/or action potentials in the distal dendrites (Miles *et al.* 1996; Tsubokawa & Ross, 1996; Kamondi *et al.* 1998). In a more co-operative mode of interaction with excitatory events, local hyperpolarization of the membrane could also remove inactivation of low threshold calcium channels (Magee *et al.* 1995) and/or sodium channels, facilitating the ability of dendrites to generate dendritic spikes. Distal dendrites have been shown to play an important role in calcium electrogenesis and action potential generation (Kamondi *et al.* 1998). At the network level, the strongly facilitating input of O-LMCs predicts their activation by repetitive firing of pyramidal cells (Lacaille *et al.* 1987; Ali & Thomson, 1998) occurring during theta frequency EEG activity. Rhythmically activated O-LM and O-BiCs may co-operate with theta frequency inputs by synchronising oscillations in dendrites, as do AACs and BCs through perisomatic terminals (Cobb *et al.* 1995; see Freund & Buzsaki, 1996). In behaving animals, pyramidal cells fire repetitive action potentials during theta activity in precise phase relationship to the population activity (O'Keefe & Recce, 1993). Phase coding by place cells may be substantially assisted and enhanced by O-LMC and O-BiC feed-back circuits to pyramidal cells, governing the timing of entorhinal and Schaffer collateral/commissural inputs, respectively, as a function of pyramidal cell output.

Alger, B. E. & Nicoll, R. A. (1982). Pharmacological evidence for two kinds of GABA receptor on rat hippocampal pyramidal cells studied *in vitro*. *Journal of Physiology* **328**, 125–141.

Ali, A. B., Deuchars, J., Pawelzik, H. & Thomson, A. M. (1998). CA1 pyramidal to basket and bistratified cell EPSPs: dual intracellular recordings in rat hippocampal slices. *Journal of Physiology* **507**, 201–217.

Ali, A. B. & Thomson, A. M. (1998). Facilitating pyramid to horizontal oriens-alveus interneurone inputs: dual intracellular recordings in slices of rat hippocampus. *Journal of Physiology* **507**, 185–199.

Andersen, P., Eccles, J. C. & Loyning, Y. (1963). Recurrent inhibition in the hippocampus with identification of the inhibitory cell and its synapses. *Nature* **198**, 540–542.

Auger, C., Kondo, S. & Marty, A. (1998). Multivesicular release of single functional synaptic sites in cerebellar stellate and basket cells. *Journal of Neuroscience* **18**, 4532–4547.

Banks, M. I., Li, T. B. & Pearce, R. A. (1998). The synaptic basis of $GABA_A$, slow. *Journal of Neuroscience* **18**, 1305–1317.

Baude, A., Nusser, Z., Roberts, J. D. B., Mulvihill, E., McIlhinney, R. A. J. & Somogyi, P. (1993). The metabotropic glutamate receptor (mGluR1α) is concentrated at perisynaptic membrane of neuronal subpopulations as detected by immunogold reaction. *Neuron* **11**, 771–787.

Blasco-Ibanez, J. M. & Freund, T. F. (1995). Synaptic input of horizontal interneurons in stratum oriens of the hippocampal CA1 subfield: structural basis of feed-back activation. *European Journal of Neuroscience* **7**, 2170–2180.

Bragin, A., Jando, G., Nadasdy, Z., Hetke, J., Wise, K. & Buzsaki, G. (1995). Gamma (40–100 Hz) oscillation in the hippocampus of the behaving rat. *Journal of Neuroscience* **15**, 47–60.

Buhl, E. H., Halasy, K. & Somogyi, P. (1994). Diverse sources of hippocampal unitary inhibitory postsynaptic potentials and the number of synaptic release sites. *Nature* **368**, 823–828.

Buzsaki, G. & Eidelberg, E. (1981). Commissural projection to the dentate gyrus of the rat: evidence for feed-forward inhibition. *Brain Research* **230**, 346–350.

Buzsaki, G., Penttonen, M., Nadasdy, Z. & Bragin, A. (1996). Pattern and inhibition-dependent invasion of pyramidal cell dendrites by fast spikes in the hippocampus in vivo. *Proceedings of the National Academy of Sciences of the USA* **93**, 9921–9925.

Cobb, S. R., Buhl, E. H., Halasy, K., Paulsen, O. & Somogyi, P. (1995). Synchronization of neuronal activity in hippocampus by individual GABAergic interneurons. *Nature* **378**, 75–78.

Csicsvari, J., Hirase, H., Czurko, A., Mamiya, A. & Buzsaki, G. (1999). Oscillatory coupling of hippocampal pyramidal cells and interneurons in the behaving rat. *Journal of Neuroscience* **19**, 274–287.

Davies, C. H., Davies, S. N. & Collingridge, G. L. (1990). Paired-pulse depression of monosynaptic GABA-mediated inhibitory postsynaptic responses in rat hippocampus. *Journal of Physiology* **424**, 513–531.

Freund, T. F. & Buzsaki, G. (1996). Interneurons of the hippocampus. *Hippocampus* **6**, 347–470.

Hajos, N. & Mody, I. (1997). Synaptic communication among hippocampal interneurons: properties of spontaneous IPSCs in morphologically identified cells. *Journal of Neuroscience* **17**, 8427–8442.

Hajos, N., Papp, E. C., Acsady, L., Levey, A. I. & Freund, T. F. (1998). Distinct interneuron types express M2 muscarinic receptor immunoreactivity on their dendrites or axon terminals in the hippocampus. *Neuroscience* **82**, 355–376.

Jones, M. V. & Westbrook, G. L. (1997). Shaping of IPSCs by endogenous calcineurin activity. *Journal of Neuroscience* **17**, 7626–7633.

Kamondi, A., Acsady, L. & Buzsaki, G. (1998). Dendritic spikes are enhanced by cooperative network activity in the intact hippocampus. *Journal of Neuroscience* **18**, 3919–3928.

Kandel, E. R., Spencer, W. A. & Brinley, F. J. (1961). Electrophysiology of hippocampal neurons I. Sequential invasion and synaptic organization. *Journal of Neurophysiology* **24**, 225–242.

Katona, I., Acsady, L. & Freund, T. F. (1999). Postsynaptic targets of somatostatin-immunoreactive interneurons in the rat hippocampus. *Neuroscience* **88**, 37–55.

Kawaguchi, Y., Katsumaru, H., Kosaka, T., Heizmann, C. W. & Hama, K. (1987). Fast spiking cells in rat hippocampus ($CA_1$ region) contain the calcium-binding protein parvalbumin. *Brain Research* **416**, 369–374.

Kosaka, T. & Hama, K. (1985). Gap junctions between non-pyramidal cell dendrites in the rat hippocampus (CA1 and CA3 regions): a combined Golgi-electron microscopy study. *Journal of Comparative Neurology* **231**, 150–161.

Lacaille, J.-C., Mueller, A. L., Kunkel, D. D. & Schwartzkroin, P. A. (1987). Local circuit interactions between oriens/alveus interneurons and CA1 pyramidal cells in hippocampal slices: electrophysiology and morphology. *Journal of Neuroscience* **7**, 1979–1993.

McBain, C. J., Dichiara, T. J. & Kauer, J. A. (1994). Activation of metabotropic glutamate receptors differentially affects two classes of hippocampal interneurons and potentiates excitatory synaptic transmission. *Journal of Neuroscience* **14**, 4433–4445.

Maccaferri, G. & McBain, C. J. (1995). Passive propagation of LTD to stratum oriens-alveus inhibitory neurons modulates the temporoammonic input to the hippocampal CA1 region. *Neuron* **15**, 137–145.

Maccaferri, G. & McBain, C. J. (1996). The hyperpolarization-activated current ($I_h$) and its contribution to pacemaker activity in rat CA1 hippocampal stratum oriens-alveus interneurones. *Journal of Physiology* **497**, 119–130.

Magee, J. C., Christofi, G., Miyakawa, H., Christie, B., Lasser-Ross, N. & Johnston, D. (1995). Subthreshold synaptic activation of voltage-gated $Ca^{2+}$ channels mediates a localized $Ca^{2+}$ influx into the dendrites of hippocampal pyramidal neurons. *Journal of Neurophysiology* **74**, 1335–1342.

Mann-Metzer, P. & Yarom, Y. (1999). Electrotonic coupling interacts with intrinsic properties to generate synchronized activity in cerebellar networks of inhibitory interneurons. *Journal of Neuroscience* **19**, 3296–3306.

Miles, R., Toth, K., Gulyas, A. I., Hajos, N. & Freund, T. F. (1996). Differences between somatic and dendritic inhibition in the hippocampus. *Neuron* **16**, 815–823.

Miles, R. & Wong, R. K. S. (1984). Unitary inhibitory synaptic potentials in the guinea-pig hippocampus *in vitro*. *Journal of Physiology* **356**, 97–113.

Morino, P., Herrera-Marschitz, M., Castel, M. N., Ungerstedt, U., Varro, A., Dockray, G. & Hokfelt, T. (1994). Cholecystokinin in cortico-striatal neurons in the rat: immunohistochemical studies at the light and electron microscopical level. *European Journal of Neuroscience* **6**, 681–692.

Naus, C. C. G., Morrison, J. H. & Bloom, F. E. (1988). Development of somatostatin-containing neurons and fibers in the rat hippocampus. *Developmental Brain Research* **40**, 113–121.

O'Keefe, J. & Recce, M. L. (1993). Phase relationship between hippocampal place units and the EEG theta rhythm. *Hippocampus* **3**, 317–330.

Ouardouz, M. & Lacaille, J. C. (1997). Properties of unitary IPSCs in hippocampal pyramidal cells originating from different types of interneurons in young rats. *Journal of Neurophysiology* **77**, 1939–1949.

Pearce, R. A. (1993). Physiological evidence for two distinct $GABA_A$ responses in rat hippocampus. *Neuron* **10**, 189–200.

Pearce, R. A., Grunder, S. D. & Faucher, L. D. (1995). Different mechanisms for use-dependent depression of two $GABA_A$-mediated IPSCs in rat hippocampus. *Journal of Physiology* **484**, 425–435.

Peters, A. & Palay, S. L. (1996). The morphology of synapses. *Journal of Neurocytology* **25**, 687–700.

Poisbeau, P., Cheney, M. C., Browning, M. D. & Mody, I. (1999). Modulation of synaptic $GABA_A$ receptor function by PKA and PKC in adult hippocampal neurons. *Journal of Neuroscience* **19**, 674–683.

Ramon y Cajal, S. (1893). Estructura del asta de ammon y fascia dentata. *Anales de Sociedad espanola Historia natural* **22**, 53–114.

Reyes, A., Lujan, R., Rozov, A., Burnashev, N., Somogyi, P. & Sakmann, B. (1998). Target-cell-specific facilitation and depression in neocortical circuits. *Nature Neuroscience* **1**, 279–285.

Sik, A., Penttonen, M., Ylinen, A. & Buzsaki, G. (1995). Hippocampal CA1 interneurons: an in vivo intracellular labeling study. *Journal of Neuroscience* **15**, 6651–6665.

Soltesz, I., Smetters, D. K. & Mody, I. (1995). Tonic inhibition originates from synapses close to the soma. *Neuron* **14**, 1273–1283.

Somogyi, P., Hodgson, A. J., Smith, A. D., Nunzi, M. G., Gorio, A. & Wu, J. (1984). Different populations of GABAergic neurons in the visual cortex and hippocampus of cat contain somatostatin- or cholecystokinin-immunoreactive material. *Journal of Neuroscience* **4**, 2590–2603.

Somogyi, P., Tamas, G., Lujan, R. & Buhl, E. H. (1998). Salient features of synaptic organisation in the cerebral cortex. *Brain Research Reviews* **26**, 113–135.

Spruston, N., Jaffe, D. B., Williams, S. H. & Johnston, D. (1993). Voltage- and space-clamp errors associated with the measurement of electrotonically remote synaptic events. *Journal of Neurophysiology* **70**, 781–802.

Thomson, A. M., West, D. C., Hahn, J. & Deuchars, J. (1996). Single axon IPSPs elicited in pyramidal cells by three classes of interneurones in slices of rat neocortex. *Journal of Physiology* **496**, 81–102.

Tsubokawa, H. & Ross, W. N. (1996). IPSPs modulate spike backpropagation and associated $[Ca^{2+}]_i$ changes in the dendrites of hippocampal CA1 pyramidal neurons. *Journal of Neurophysiology* **76**, 2896–2906.

Williams, S. R., Buhl, E. H. & Mody, I. (1998). The dynamics of synchronized neurotransmitter release determined from compound spontaneous IPSCs in rat dentate granule neurones *in vitro*. *Journal of Physiology* **510**, 477–497.

Yanovsky, Y., Sergeeva, O. A., Freund, T. F. & Haas, H. L. (1997). Activation of interneurons at the stratum oriens/alveus border suppresses excitatory transmission to apical dendrites in the CA1 area of the mouse hippocampus. *Neuroscience* **77**, 87–96.

**Acknowledgements**

We would like to thank Drs E. Buhl, N. Kogo, I. Mody, Z. Nusser and O. Paulsen for constructive criticisms of a previous version of the manuscript, and Mrs Laura Lyford for editorial assistance. We also thank Dr A. Buchan at the Department of Physiology, University of British Columbia, Vancouver, Canada, for the generous gift of monoclonal antibodies to somatostatin, Dr K. G. Baimbridge, Department of Physiology, University of British Columbia, Vancouver, Canada, for the rabbit antibodies to parvalbumin, Dr J. Dempster, University of Strathclyde for providing us with the WCP analysis package and Miss Z. Ahmad and Mr P. Jays for excellent assistance. This work was also supported by a European Commission Shared Cost RTD Programme (no. BIO4CT96-0585).

**Correspondence**

G. Maccaferri: gmaccaf@emory.edu

P. Somogyi: peter.somogyi@pharmacology.oxford.ac.uk

**Authors' present addresses**

G. Maccaferri: Department of Pharmacology, Emory University School of Medicine, Atlanta, GA, USA.

P. Szucs: Department of Anatomy, Histology and Embryology, University Medical School, Debrecen, Hungary.

C. Cottingham: The Newman Partnership SCITT, All Hallows High School, Preston, UK.